

Bayesian Inference of Vector Autoregressions with Tensor Decompositions

Yiyong Luo* Jim E. Griffin†

Department of Statistical Science, University College London, WC1E 6BT, UK

ABSTRACT

Vector autoregressions (VARs) are popular in analyzing economic time series. However, VARs can be over-parameterized if the numbers of variables and lags are moderately large. Tensor VAR, a recent solution to over-parameterization, treats the coefficient matrix as a third-order tensor and estimates the corresponding tensor decomposition to achieve parsimony. In this paper, we employ the Tensor VAR structure with a CANDECOMP/PARAFAC (CP) decomposition and conduct Bayesian inference to estimate parameters. Firstly, we determine the rank by imposing the Multiplicative Gamma Prior to margins, i.e. elements in the decomposition, and accelerate the computation with an adaptive inferential scheme. Secondly, to obtain interpretable margins, we propose an interweaving algorithm to improve the mixing of margins. In the application of the US macroeconomic data, our models outperform standard VARs in point and density forecasting and yield a summary of the US economic dynamic.

Keywords: Ancillarity-sufficiency interweaving strategy (ASIS), High-dimensional data, Markov chain Monte Carlo (MCMC), Increasing shrinkage prior

*Corresponding author at Department of Statistical Science, University College London, WC1E 6BT, UK.

E-mail address: yiyong.luo.20@ucl.ac.uk

†E-mail address: j.griffin@ucl.ac.uk

1 Introduction

Vector autoregression (VAR) is a multivariate time series model that describes the linear interrelationship of data. Since the advocacy of [Sims \(1980\)](#), VAR is a widely used tool for modelling macroeconomic variables, which are known to be temporally dependent with each other. As suggested in [Korobilis and Pettenuzzo \(2019\)](#), [Carriero et al. \(2019\)](#), [Bańbura et al. \(2010\)](#) and [Giannone et al. \(2015\)](#), to name a few, applying VARs to a large set of variables is advantageous for forecasting and structural analysis. However, one must solve over-parameterization, i.e. the number of parameters is relatively high to the sample size, in order to achieve success in modelling large VARs. Over-parameterization is especially an issue for macroeconomic data due to the low frequency in data collection.

Methodologies to solve over-parameterization in VARs can be divided into *sparse-* and *dense-*modelling streams, according to [Ng \(2013\)](#). The sparse stream assumes that only a small set of predictors are important to model the time series of each variable. For example, [Hsu et al. \(2008\)](#) proposed using the Lasso penalty ([Tibshirani, 1996](#)) for VARs, which was subsequently developed by [Song and Bickel \(2011\)](#), [Shojaie and Michailidis \(2010\)](#) and [Nicholson et al. \(2020\)](#). The dense stream relies on an opposite assumption to its sparse-modelling counterpart: all predictors could be important, but their corresponding parameters may have small magnitudes. Shrinkage priors, including the Minnesota-type priors ([Litterman et al., 1979](#); [Litterman, 1986](#); [Doan et al., 1984](#)), Stochastic Search Variable Selection (SSVS) ([George et al., 2008](#)), and global-local shrinkage priors ([Huber and Feldkircher, 2019](#); [Follett and Yu, 2019](#); [Huber et al., 2019](#); [Gruber and Kastner, 2022](#)) dominate the dense-modelling stream in a VAR framework. An alternative methodology in this stream, called reduced-rank VAR ([Velu et al., 1986](#); [Carriero et al., 2011](#)), assumes that the coefficient matrix has a low rank and one can decompose this matrix to achieve parsimony. A more recent and related technique, referred to as Tensor VAR, treats the coefficient matrix as a third-order tensor and infers this tensor by its low-rank decomposition. [Wang et al. \(2021\)](#) was the first to

introduce Tensor VAR and this technique has been developed in [Zhang et al. \(2021\)](#) and [Fan et al. \(2022\)](#).

In this paper, we contribute to the dense-modelling stream by employing the Tensor VAR structure with a CANDECOMP/PARAFAC (CP) decomposition ([Kiers, 2000](#)) and conducting Bayesian inference to estimate parameters. The motivation of choosing this methodology to alleviate over-parameterization is fourfold. Firstly, recent work has questioned whether sparse-modelling is appropriate for macroeconomic data, e.g. see [Giannone et al. \(2021\)](#) for the "illusion of sparsity". Secondly, a Tensor VAR with an appropriate choice of rank is parsimonious without imposing any penalty term or shrinkage prior (although incorporating these techniques results in further parsimony). Thirdly, Tensor VAR is a useful model for explaining macroeconomic data since its reconstruction provides insights to the economy, and elements in its tensor decomposition (usually called *margins*) are interpretable as shown in [Wang et al. \(2021\)](#) and [Chen et al. \(2022\)](#). Lastly, tensor structures with Bayesian inference have been successfully applied in time series models apart from VARs. Related work includes time-varying networks ([Billio et al., 2022a](#)) and Autoregressive Tensor Processes (ART) ([Billio et al., 2022b](#)), among others.

Two challenges arise when making Bayesian inference to a Tensor VAR with a CP decomposition. The first challenge is about the inference of the rank, which is an important parameter in the CP decomposition because it controls the model flexibility. Unlike finding the rank in a matrix, there is no straightforward algorithm to determine the rank of a third-order tensor. Although existing literature gives rank values of some specified tensors, see [Kolda and Bader \(2009\)](#) and references therein, tensors for large VARs have relatively high dimensions, so they normally do not nest in these specified ones. To overcome this challenge, past literature proposed multiway Dirichlet generalized double Pareto (M-DGDP) prior ([Guhaniyogi et al., 2017](#)) and multiway stick breaking shrinkage prior ([Guhaniyogi and Spencer, 2021](#)), based on overfitted mixture models ([Rousseau and Mengersen, 2011](#)), to induce a low-rank structure in the CP decomposition and inferred the rank *a posteriori*. Despite being a prominent method to resolve the challenge, it is computationally expensive due to the large initialization of the rank. The second challenge is to retain the interpretability of a Tensor

VAR. From a Bayesian perspective, a fundamental prerequisite for a Tensor VAR to be interpretable is the good mixing of Markov chains of margins, but this prerequisite cannot be achieved using the traditional MCMC scheme due to the indeterminacy of the CP decomposition. One solution is to impose restrictions to margins as in [Zhou et al. \(2013\)](#), whereas solutions in unrestricted parameter space have not been explored yet.

We tackle the above challenges with two respective contributions. Our first contribution is to infer the rank through the help of an increasing shrinkage prior. We impose the Multiplicative Gamma prior (MGP) ([Bhattacharya and Dunson, 2011](#)) to margins and use an adaptive inferential scheme to infer these margins, and subsequently the rank. This idea is closely related to the recent work in [Fan et al. \(2022\)](#), but our prior and the criterion in the adaptive inference are different from theirs. In our second contribution, we propose a Gibbs sampler including a variant of Ancillarity-Sufficiency Interweaving Strategy (ASIS) ([Yu and Meng, 2011](#)) with three interweaving steps, inspired by the ASIS for factor models ([Kastner et al., 2017](#)). Besides the interweaving strategy, margins are divided into three blocks during inference to reduce dependence between margins. Even if the mixing of margins is not essential in some instances, e.g. one does not interpret margins and only regards the mixing of entries in tensor itself as important, this contribution is still beneficial because achieving good mixing of margins provides a solid foundation for entries in the coefficient matrix to mix well.

We examine the utility of Tensor VARs through two US macroeconomic data sets with medium and large sizes. We consider two specifications of Tensor VARs that treat the coefficient matrix in two ways: (1) the matricization of a third-order tensor; and (2) a sum of the matricization of a third-order tensor and a matrix with only non-zero entries for own lags. The first one corresponds to the original Tensor VAR idea ([Wang et al., 2021](#)), and the second one accommodates the feature of Minnesota-type priors, i.e. the own lags of a variable are more informative than lags of other dependent variables. In point and density forecasting, these two Tensor VARs obtain the best results for joint forecasts and are competitive to standard VARs with a range of standard prior choices. We demonstrate how to interpret margins by applying our model to the whole large-scale data and constructing factors as linear combinations of lagged data. The Tensor VAR can effectively

reduce the number of parameters, and factors constructed can summarize the dynamics of the data set. Although the additional own-lag matrix in the second Tensor VAR structure introduces more parameters than the first one, this matrix allows us to infer a lower rank in general and focuses the tensor on exploring the cross-lag effects.

The paper is organized as follows. Section 2 explains the Tensor VAR and its interpretation. Section 3 provides the MCMC schemes. Section 4 shows results from simulation experiments. Section 5 presents the forecasting performance and interpretation of Tensor VARs. Section 6 concludes the paper.

2 Tensor VAR

2.1 Model Specification

Let $\mathbf{y}_t \in \mathbb{R}^N$ be the t -th observation in a multivariate time series. A P -order VAR model, $\text{VAR}(P)$, describes the linear relation between \mathbf{y}_t and its lags with transition matrices $\mathbf{A}_1, \dots, \mathbf{A}_P \in \mathbb{R}^{N \times N}$ by

$$\mathbf{y}_t = \mathbf{A}_1 \mathbf{y}_{t-1} + \dots + \mathbf{A}_P \mathbf{y}_{t-P} + \boldsymbol{\epsilon}_t = \mathbf{A} \mathbf{x}_t + \boldsymbol{\epsilon}_t, \quad (2.1)$$

where $t = 1 \dots T$, $\mathbf{A} = (\mathbf{A}_1, \dots, \mathbf{A}_P)$ is an N -by- NP coefficient matrix linearly connecting \mathbf{y}_t and its lags, $\mathbf{x}_t = (\mathbf{y}'_{t-1}, \dots, \mathbf{y}'_{t-P})' \in \mathbb{R}^{NP}$. The error term $\boldsymbol{\epsilon}_t$ follows a multivariate normal distribution with zero mean and a time-varying covariance matrix $\boldsymbol{\Omega}_t$. In this paper, we factorize $\boldsymbol{\Omega}_t$ according to Cogley and Sargent (2005), i.e. $\boldsymbol{\Omega}_t = \mathbf{H}^{-1} \mathbf{S}_t (\mathbf{H}^{-1})'$, where \mathbf{H}^{-1} is a lower triangular matrix with ones as diagonal entries, and \mathbf{S}_t is a time-varying diagonal matrix with diagonal terms $(s_{t,1}, \dots, s_{t,N})$.

To fit the VAR model, we must estimate the N^2P parameters in \mathbf{A} and parameters for the covariance matrix $\boldsymbol{\Omega}_t$. The number of coefficients grows quadratically as the number of time series increases, thus VARs can become easily overparameterized. We address this problem by achieving parsimony of \mathbf{A} through tensor decomposition, in the spirit of Wang et al. (2021). Specifically, rather than modelling the \mathbf{A} directly, we model a third-order tensor $\mathcal{A} \in \mathbb{R}^{N \times N \times P}$, where $\mathcal{A}_{i_1, i_2, p}$ corresponds to the (i_1, i_2) entry in \mathbf{A}_p . The model in (2.1) can be written in terms of the tensor \mathcal{A}

to give

$$\mathbf{y}_t = \mathcal{A}_{(1)}\mathbf{x}_t + \boldsymbol{\epsilon}_t, \quad (2.2)$$

where $\mathcal{A}_{(1)} = \mathbf{A}$ is the mode-1 matricization of \mathcal{A} , with the i_1 -th row as the vectorization of $\mathcal{A}_{(i_1, \cdot, \cdot)}$.

So far, the number of entries in \mathcal{A} is the same as that in \mathbf{A} , but we can decompose \mathcal{A} via a rank- R CP decomposition,

$$\mathcal{A} = \sum_{r=1}^R \mathcal{A}^{(r)} = \sum_{r=1}^R \boldsymbol{\beta}_1^{(r)} \circ \boldsymbol{\beta}_2^{(r)} \circ \boldsymbol{\beta}_3^{(r)}, \quad (2.3)$$

where $\mathcal{A}^{(r)}$ is a third-order tensor with the same dimension as \mathcal{A} , for $r = 1, \dots, R$; $\boldsymbol{\beta}_1^{(r)}, \boldsymbol{\beta}_2^{(r)} \in \mathbb{R}^N$ and $\boldsymbol{\beta}_3^{(r)} \in \mathbb{R}^P$ are called margins of \mathcal{A} , and they are connected by \circ such that $\boldsymbol{\beta}_{1,i_1}\boldsymbol{\beta}_{2,i_2}\boldsymbol{\beta}_{3,i_3}$ is the (i_1, i_2, i_3) entry in $\mathcal{A}^{(r)}$, for $i_1, i_2 = 1, \dots, N$ and $i_3 = 1, \dots, P$. We define the notation $\mathbf{B}_j = (\boldsymbol{\beta}_j^{(1)}, \dots, \boldsymbol{\beta}_j^{(R)}) \in \mathbb{R}^{I_j \times R}$, for $j = 1, 2, 3$, $I_1 = I_2 = N$ and $I_3 = P$, then the tensor \mathcal{A} decomposed by $\mathbf{B}_1, \mathbf{B}_2, \mathbf{B}_3$ is written as $\mathcal{A} = \llbracket \mathbf{B}_1, \mathbf{B}_2, \mathbf{B}_3 \rrbracket_{\text{CP}}$, for the sake of brevity. Another useful representation of the margins is $\mathbf{B} = (\mathbf{B}'_1, \mathbf{B}'_2, \mathbf{B}'_3)' \in \mathbb{R}^{(2N+P) \times R}$ to which we refer as a *tensor matrix*, then $\mathcal{A}^{(r)}$ is constructed by margins in the r -th column of \mathbf{B} . With an upper bound $N^2P/(2N+P)$ of R , the number of parameters reduces from N^2P in the coefficient matrix to $(2N+P)R$ in \mathbf{B} , so a low-rank structure in the CP decomposition alleviates over-parameterization.

The CP decomposition is only identified up to scaling and permutation because $\mathcal{A} = \llbracket \mathbf{B}_1, \mathbf{B}_2, \mathbf{B}_3 \rrbracket_{\text{CP}} = \llbracket \tilde{\mathbf{B}}_1, \tilde{\mathbf{B}}_2, \tilde{\mathbf{B}}_3 \rrbracket_{\text{CP}}$, if $\tilde{\mathbf{B}}_j$ comes from the following transformations for $j = 1, 2, 3$:

1. Scaling: $\tilde{\mathbf{B}}_j = \mathbf{B}_j \mathbf{R}_j$, and \mathbf{R}_j is an R -by- R diagonal matrix satisfying $\prod_{j=1}^J \mathbf{R}_{j,(r,r)} = 1$ for $r = 1, \dots, R$, where $\mathbf{R}_{j,(r,r)}$ is the r -th diagonal term in \mathbf{R}_j .
2. Permutation: $\tilde{\mathbf{B}}_j = \mathbf{B}_j \boldsymbol{\Pi}$ for an arbitrary R -by- R column-wise permutation matrix $\boldsymbol{\Pi}$.

This indeterminacy will play an important role in our algorithm in Section 3.2.2.

The model in (2.2) represents the original Tensor VAR (Wang et al., 2021), which does not distinguish between the own-lag and cross-lag effects. In Section 5.4, we empirically find that introducing this distinction allows us to infer a lower rank in a stable way, so we build an extension of (2.2), called Own-lag Tensor VAR, following the assumption of the Minnesota-type priors - the

own-lag effects are more powerful than the cross-lag effects. In particular, we add a matrix \mathbf{D} , the concatenation of P N -dimensional diagonal matrices, to give

$$\mathbf{y}_t = \mathcal{A}_{(1)}\mathbf{x}_t + \mathbf{D}\mathbf{x}_t + \boldsymbol{\epsilon}_t, \quad (2.4)$$

so \mathbf{D} can only affect entries corresponding to own lags.

2.2 Model Interpretation

The Own-lag Tensor VAR connects $\mathbf{y}_t^* = \mathbf{y}_t - \mathbf{D}\mathbf{x}_t$ with past information through $\mathbf{B}_1, \mathbf{B}_2, \mathbf{B}_3$ in the following reconstruction,

$$\mathbf{y}_t^* = \mathbf{B}_1 \mathcal{I}_{(1)} \text{vec}(\mathbf{B}'_2 \mathbf{X}_t \mathbf{B}_3) + \boldsymbol{\epsilon}_t \quad (2.5)$$

$$= \sum_{r=1}^R \mathbf{B}_{1,(\cdot,r)} \sum_{i_2=1}^N \sum_{i_3=1}^P \boldsymbol{\beta}_{2,i_2}^{(r)} \boldsymbol{\beta}_{3,i_3}^{(r)} \mathbf{y}_{t-i_3,i_2} + \boldsymbol{\epsilon}_t, \quad (2.6)$$

where $\mathcal{I}_{(1)} \in \mathbb{R}^{R \times R^2}$ is the mode-1 matricization of a third-order superdiagonal tensor \mathcal{I} (see supplementary Appendix A for a detailed description), $\mathbf{X}_t = (\mathbf{y}_{t-1}, \dots, \mathbf{y}_{t-P})$, $\text{vec}(\cdot)$ is the vectorization operation which transforms $\mathbf{B}'_2 \mathbf{X}_t \mathbf{B}_3 \in \mathbb{R}^{R \times R}$ to an R^2 -dimensional vector, $\mathbf{B}_{1,(\cdot,r)}$ is the r -th column of \mathbf{B}_1 , $\boldsymbol{\beta}_{2,i_2}^{(r)}, \boldsymbol{\beta}_{3,i_3}^{(r)}$ are the (i_2, r) and (i_3, r) entries of \mathbf{B}_2 and \mathbf{B}_3 , respectively, \mathbf{y}_{t-i_3,i_2} is the i_2 -th entry in \mathbf{y}_{t-i_3} . Note that this reconstruction also holds for (2.2) because it is a specification of (2.4) with \mathbf{D} being a zero matrix.

Following Wang et al. (2021), we can relate (2.5) to a factor model (Stock and Watson, 2005, 2011), where \mathbf{B}_1 is the factor loading and $\mathcal{I}_{(1)} \text{vec}(\mathbf{B}'_2 \mathbf{X}_t \mathbf{B}_3)$ contains R observable factors. Since the i_1 -th row in \mathbf{B}_1 describes the linear relationship between \mathbf{y}_{t,i_1} and factors, for $i_1 = 1, \dots, N$, we refer to \mathbf{B}_1 as "response loading". The formation of factors describes how past information is combined. We look at the last three terms in (2.6) to understand this formation. If $\boldsymbol{\beta}_{2,i_2}^{(r)} = 0$, the r -th factor will not contain information from any lagged values of \mathbf{y}_{t,i_2} . Similarly, $\boldsymbol{\beta}_{3,i_3}^{(r)} = 0$ results to no information about the i_3 -th lag of \mathbf{y}_t in the r -th factor. Therefore, the i_2 -th row of \mathbf{B}_2 contains the effect from the i_2 -th variable to \mathbf{y}_t , and the i_3 -th row of \mathbf{B}_3 is related to the effect from the i_3 -th lag to \mathbf{y}_t . This interpretation was also discussed in Wang et al. (2021), who called \mathbf{B}_2 and \mathbf{B}_3 "predictor loading" and "temporal loading", respectively.

Another way to explain the CP decomposition in the Tensor VAR is that it separates the lag effect from the variable-wise effect because it decomposes \mathbf{A}_p as

$$\mathbf{A}_p = \sum_{r=1}^R (\boldsymbol{\beta}_1^{(r)} \circ \boldsymbol{\beta}_2^{(r)}) \boldsymbol{\beta}_{3,p}^{(r)}.$$

The first two vectors $\boldsymbol{\beta}_1^{(r)}$ and $\boldsymbol{\beta}_2^{(r)}$ (for $r = 1, \dots, R$) do not depend on the index of \mathbf{A}_p , suggesting that all transition matrices share these vectors. The only difference among these transition matrices reflects on the different entries in $\boldsymbol{\beta}_3^{(r)}$.

3 Bayesian Inference

3.1 Prior Specification

As mentioned in Section 2.1, we aim to impose a prior on the tensor matrix \mathbf{B} and then induce the model to favour low-rank structure. A particular prior choice that meets our requirement is the MGP because it possesses the increasing shrinkage property, enabling margins with higher column index to have higher degrees of shrinkage. As a result, the rank can be lowered if some columns in \mathbf{B} have magnitudes negligibly small. To be specific, a margin $\boldsymbol{\beta}_{j,i_j}^{(r)}$ (the (i_j, r) entry of \mathbf{B}_j) follows the prior below for $j = 1, 2, 3, r = 1, \dots, R, i_1, i_2 = 1, \dots, N$ and $i_3 = 1, \dots, P$:

$$\begin{aligned} \boldsymbol{\beta}_{j,i_j}^{(r)} &\sim \mathcal{N}\left(0, (\sigma_{j,i_j}^{(r)})^2\right), (\sigma_{j,i_j}^{(r)})^2 = \phi_{(r,j,i_j)}^{-1} \tau_r^{-1}, \\ \phi_{(r,j,i_j)} &\sim \text{Gamma}(\nu/2, \nu/2), \tau_r = \prod_{l=1}^r \delta_l, \end{aligned}$$

$$\delta_1 \sim \text{Gamma}(a_1, 1), \delta_l \sim \text{Gamma}(a_2, 1), 1 < l < R,$$

where $\phi_{(r,j,i_j)}$ is a local parameter for the margin with the same index. We store all these local parameters in a matrix $\boldsymbol{\Phi}$ in which each entry corresponds to the local parameter of an entry in the tensor matrix \mathbf{B} with the same indices. The increasing shrinkage property is induced by τ_r since $\mathbb{E}(\tau_r) = \prod_{l=1}^r \mathbb{E}(\delta_l) = a_1 a_2^{r-1}$ increases with r , when $a_2 > 1$. Hyperparameter ν is set to be known, and a_1 and a_2 will be inferred with Gamma priors. Durante (2017) showed that both $\mathbb{E}(\tau_r)$ and $\mathbb{E}(\tau_r^{-1})$ increase with r when $1 < a_2 < 2$. This result means that the MGP has the increasing

shrinkage property only when $a_2 > 2$. Thus, we set priors for a_1 and a_2 as Gamma(5,1) to have the increasing shrinkage property with a high probability.

Apart from the shrinkage prior for \mathbf{B} , we follow priors in [Huber and Feldkircher \(2019\)](#) for \mathbf{H} and \mathbf{S}_t . Each non-zero off-diagonal entry in \mathbf{H} follows a variant of the normal-gamma prior ([Brown and Griffin, 2010](#)),

$$\mathbf{H}_{i,j} \sim \mathcal{N}\left(0, (2/\lambda_h^2)\psi_h^{(i,j)}\right), \psi_h^{(i,j)} \sim \text{Gamma}(a_h, a_h), \text{ for } i = 1, \dots, N \text{ and } j < i,$$

where λ_h^2 is the global parameter which controls the overall shrinkage and follows Gamma(0.01,0.01) prior, $\psi_h^{(i,j)}$ allows flexibility locally, hyperparameter a_h follows an exponential prior with parameter 1.

The sequence $s_{1,n}, \dots, s_{T,n}$ evolves with a stochastic volatility model ([Jacquier et al., 2002](#); [Kim et al., 1998](#)). The logarithm of $s_{t,n}$ follows

$$\begin{aligned} \ln(s_{t,n}) \mid \ln(s_{t-1,n}), \mu_n, \psi_n, \sigma_n &\sim \mathcal{N}\left(\mu_n + \psi_n (\ln(s_{t-1,n}) - \mu_n), \sigma_n^2\right), \\ \ln(s_{0,n}) \mid \mu_n, \psi_n, \sigma_n &\sim \mathcal{N}\left(\mu_n, \sigma_n^2/(1 - \psi_n^2)\right). \end{aligned}$$

Priors of hyperparameters, $\mu_n, \psi_n, \sigma_n^2$, are the same as those in [Kastner and Frühwirth-Schnatter \(2014\)](#), for $n = 1, \dots, N$. We impose $\mathcal{N}(0, 100)$ to μ_n , Beta(5, 1.5) to $\frac{1+\psi_n}{2}$ and Gamma(1/2, 1/2) to σ_n^2 . The prior for σ_n^2 implies that σ_n follows a standard normal distribution.

In the case of (2.4), we impose the same normal-gamma prior to each non-zero entry in \mathbf{D} . Let $d_{i,p}$ denote the own-lag coefficient for the p -th lag of the i -th response, then its prior is written as

$$d_{i,p} \sim \mathcal{N}\left(0, (2/\lambda_d^2)\psi_d^{(i,p)}\right), \psi_d^{(i,p)} \sim \text{Gamma}(a_d, a_d), \text{ for } i = 1, \dots, N \text{ and } p = 1, \dots, P.$$

Priors of hyperparameters are the same as those for lower triangular matrix \mathbf{H} . All the full conditionals and their derivation can be found in supplementary Appendix B.

3.2 MCMC Scheme

3.2.1 An Overview of MCMC Scheme

To illustrate the strengths of our MCMC scheme, we contrast it with the widely-used MCMC scheme for tensor-structured models. In the traditional scheme (Guhaniyogi et al., 2017; Billio et al., 2022b; Zhang et al., 2021; Fan et al., 2022), $\beta_j^{(r)}$ is sampled from $p\left(\beta_j^{(r)} \mid \beta_{-j}^{(r)}, \mathbf{B}_{(\cdot, -r)}, \mathbf{y}_{1:T}, (\sigma_j^{(r)})^2\right)$, for $r = 1, \dots, R$ and $j = 1, \dots, J$ (J is 3 in our case), where $\beta_{-j}^{(r)}$ contains all $\beta_{j'}^{(r)}$ with $j' \neq j$, $\mathbf{B}_{(\cdot, -r)}$ is \mathbf{B} discarding its r -th column, $(\sigma_j^{(r)})^2$ has all prior variance corresponding to $\beta_j^{(r)}$. These full conditionals are then incorporated into a usual Gibbs sampler, so each $\beta_j^{(r)}$ sampled depends on other margins, and in turn, other margins are sampled given $\beta_j^{(r)}$ and other parameters. The rank R is fixed to a large value during the inference and can be determined to a smaller value *a posteriori*. This MCMC scheme neglects the mixing issue of margins because authors are more interested in the tensor itself, so they pay more attention to the mixing of the tensor elements, rather than the margins. We consider the mixing of margins as an important aspect for two reasons. First, Tensor VARs are potentially interpretable, as shown in Wang et al. (2021) and Chen et al. (2022), and discussed in Section 2.2. Second, as the literature on Tensor VARs grows, one cannot guarantee that the margins in a more complex model, e.g. including time-varying margins, still mix well. Apart from the mixing issue, it is computationally expensive to infer the rank using the traditional MCMC scheme since it assumes R to be fixed during the inference. To solve the issues aforementioned, we differ our MCMC scheme in three aspects.

Firstly, we reduce the dependence between columns within \mathbf{B}_j , for $j = 1, 2, 3$, by introducing a blocked sampler, which divides margins into three blocks according to the three loadings mentioned in Section 2.2. This block sampler is feasible because a Tensor VAR can be written as:

$$\mathbf{y}_t^* = \left(\mathbf{x}_t' (\mathbf{B}_3 \otimes \mathbf{B}_2) \mathbf{I}'_{(1)} \otimes \mathbf{I}_N \right) \text{vec}(\mathbf{B}_1) + \boldsymbol{\epsilon}_t \quad (3.1)$$

$$= \mathbf{B}_1 \mathbf{I}_{(1)} \left((\mathbf{B}'_3 \mathbf{X}'_t) \otimes \mathbf{I}_R \right) \text{vec}(\mathbf{B}'_2) + \boldsymbol{\epsilon}_t \quad (3.2)$$

$$= \mathbf{B}_1 \mathbf{I}_{(1)} \left(\mathbf{I}_R \otimes (\mathbf{B}'_2 \mathbf{X}_t) \right) \text{vec}(\mathbf{B}_3) + \boldsymbol{\epsilon}_t, \quad (3.3)$$

where $\mathbf{I} \in \mathbb{R}^{R \times R \times R}$, $\mathbf{I}_R \in \mathbb{R}^{R \times R}$ is an identity matrix, \otimes is for the Kronecker product. Therefore, margins in one loading can be sampled jointly to reduce their dependencies on each other.

Secondly, we do *not* use a usual Gibbs sampler to sample loadings. Instead, we introduce a variant of ASIS, containing four parameterizations for tensor margins, to reduce the parameter autocorrelation during the sampling. Given a rank value in each sample iteration, the interweaving Gibbs sampler interweaves between full conditional distributions under a base parameterization and the other three.

Lastly, the rank R in our case is adaptively inferred similarly to [Bhattacharya and Dunson \(2011\)](#) to speed up computation. In the following two subsections, we introduce the interweaving Gibbs sampler for a fixed rank in [3.2.2](#) and the adaptive inferential scheme of the rank in [3.2.3](#)

3.2.2 Interweaving Gibbs Sampler

In principle, we could run a standard Gibbs sampler to infer margins and other parameters, but in practice, Markov chains of margins suffer from poor mixing since these chains are highly autocorrelated. We circumvent margins with poor mixing by introducing a variant of ASIS, which unfolds its strategy from its name: sampling the same block of parameters by interweaving two sampling schemes corresponding to two data augmentations - ancillary statistic and sufficient statistic. The benefit of ASIS is that the sampling will be at least as good as the sampling from only one data augmentation; and a low correlation between these two augmentations leads to faster convergence and better mixing, compared to using either augmentation alone. Because of these benefits, ASIS has been applied to many models, including stochastic volatility ([Kastner and Frühwirth-Schnatter, 2014](#)), factor models ([Kastner et al., 2017](#)) and dynamic linear models ([Simpson, 2015](#); [Simpson et al., 2017](#)).

While the original ASIS was applied to linear mixed models and employed centred/non-centred parameterizations for these two data augmentations, our parameterizations are more related to those in [Kastner et al. \(2017\)](#) for sampling factor loadings and factors, due to the tensor structure. The tensor structure in the Tensor VAR leads to four parameterizations instead of two in [Kastner et al. \(2017\)](#).

The first parameterization, which we call the base one, is simply \mathbf{B}_1 , \mathbf{B}_2 and \mathbf{B}_3 described in Section 2.1. The remaining three parameterizations come from specifications of scaling indeterminacy described in the same section. In particular, $\mathcal{A} = \llbracket \mathbf{B}_1, \mathbf{B}_2, \mathbf{B}_3 \rrbracket_{\text{CP}} = \llbracket \mathbf{B}_1^*, \mathbf{B}_2^*, \mathbf{B}_3 \rrbracket_{\text{CP}}$ when \mathbf{B}_1^* , \mathbf{B}_2^* are transformed from

$$\mathbf{B}_1^* = \mathbf{B}_1 \mathbf{D}_1^{-1}, \mathbf{B}_2^* = \mathbf{B}_2 \mathbf{D}_1, \quad (3.4)$$

where \mathbf{D}_1 is a diagonal matrix with non-zero, non-infinite diagonal entries.

There are infinite choices of \mathbf{D}_1 to get this equivalence, but since our objective is boosting the mixing of margins, we restrict \mathbf{D}_1 to be related to \mathbf{B}_1 and \mathbf{B}_2 . After narrowing down the choices of \mathbf{D}_1 , there are still multiple available choices, including but not limited to $\mathbf{D}_1 = \text{diag}(\beta_{j,1}^{(1)}, \dots, \beta_{j,R}^{(R)})$ (diagonal entries in \mathbf{B}_1), or $\mathbf{D}_1 = \text{diag}(\beta_{j,i_j}^{(1)}, \dots, \beta_{j,i_j}^{(R)})$ (the i_j -th row in \mathbf{B}_j , for $j=1,2$). We choose $\mathbf{D}_1 = \text{diag}(\beta_{1,1}^{(1)}, \dots, \beta_{1,1}^{(R)})$ for further demonstration. This choice constrains the first row of \mathbf{B}_1^* to be ones. Other choices of \mathbf{D}_1 will be investigated in future work.

After the transformation, we are able to write the model in terms of \mathbf{B}_1^* , \mathbf{B}_2^* and \mathbf{D}_1 for the second parameterization. For $i_1, i_2 = 1, \dots, N$, we have

$$\beta_{1,1}^{*(r)} = 1, \beta_{1,i_1}^{*(r)} \sim \mathcal{N}\left(0, \left(\frac{\sigma_{1,i_1}^{(r)}}{\beta_{1,1}^{(r)}}\right)^2\right), \beta_{2,i_2}^{*(r)} \sim \mathcal{N}\left(0, \left(\sigma_{2,i_2}^{(r)} \beta_{1,1}^{(r)}\right)^2\right). \quad (3.5)$$

The above parameterization only improves the mixing of margins in \mathbf{B}_1 and \mathbf{B}_2 , so we also need a parameterization to improve the mixing of margins in \mathbf{B}_3 . An obvious choice is to pair \mathbf{B}_2 and \mathbf{B}_3 . At this point, each \mathbf{B}_j has been paired at least once, but we conjecture that an additional pair of \mathbf{B}_1 and \mathbf{B}_3 would provide better mixing than just considering three parameterizations because the mixing would be improved across margins in each pair of \mathbf{B}_j 's. Transformations of these two pairs are similar to the one for \mathbf{B}_1 and \mathbf{B}_2 ,

$$\mathbf{B}_2^{**} = \mathbf{B}_2 \mathbf{D}_2^{-1}, \mathbf{B}_3^{**} = \mathbf{B}_3 \mathbf{D}_2, \quad (3.6)$$

$$\mathbf{B}_3^{***} = \mathbf{B}_3 \mathbf{D}_3^{-1}, \mathbf{B}_1^{***} = \mathbf{B}_1 \mathbf{D}_3, \quad (3.7)$$

where \mathbf{D}_2 and \mathbf{D}_3 are diagonal matrices with non-zero, non-infinite diagonal entries.

Similarly, we choose the diagonal entries in D_2 to be the first row of B_2 , and likewise for those in D_3 (as the first row of B_3). These lead to the last two parameterizations which are presented in terms of B_2^{**}, B_3^{**}, D_2 and $B_3^{***}, B_1^{***}, D_3$, respectively. For $i_1, i_2 = 1, \dots, N, i_3 = 1, \dots, P$, we have

$$\beta_{2,1}^{**(r)} = 1, \beta_{2,i_2}^{**(r)} \sim \mathcal{N}\left(0, \left(\frac{\sigma_{2,i_2}^{(r)}}{\beta_{2,1}^{(r)}}\right)^2\right), \beta_{3,i_3}^{**(r)} \sim \mathcal{N}\left(0, \left(\sigma_{3,i_3}^{(r)} \beta_{2,1}^{(r)}\right)^2\right), \quad (3.8)$$

$$\beta_{3,1}^{***(r)} = 1, \beta_{3,i_3}^{***(r)} \sim \mathcal{N}\left(0, \left(\frac{\sigma_{3,i_3}^{(r)}}{\beta_{3,1}^{(r)}}\right)^2\right), \beta_{1,i_1}^{***(r)} \sim \mathcal{N}\left(0, \left(\sigma_{1,i_1}^{(r)} \beta_{3,1}^{(r)}\right)^2\right). \quad (3.9)$$

We need to sample margins under the four parameterizations described in each iteration. The sampling using the base parameterization is stated in supplementary Appendix B, so we focus on sampling margins under the rest three parameterizations introduced in this subsection. For $\beta_{1,1}^{(r)}$, its normal prior implies that $(\beta_{1,1}^{(r)})^2$ has a gamma prior, $\text{Gamma}\left(\frac{1}{2}, \frac{1}{2(\sigma_{1,1}^{(r)})^2}\right)$. The full conditional of $(\beta_{1,1}^{(r)})^2$ under (3.5) is a Generalized Inverse Gaussian (GIG),

$$\left(\beta_{1,1}^{(r)}\right)^2 \mid \mathbf{B}_{1,(\cdot,r)}^*, \mathbf{B}_{2,(\cdot,r)}^* \sim \text{GIG}\left(0, \sum_{i_2=1}^M \left(\frac{\beta_{2,i_2}^{*(r)}}{\sigma_{2,i_2}^{(r)}}\right)^2, \sum_{i_1=2}^M \left(\frac{\beta_{1,i_1}^{*(r)}}{\sigma_{1,i_1}^{(r)}}\right)^2 + \left(\frac{1}{\sigma_{1,1}^{(r)}}\right)^2\right), \quad (3.10)$$

where a variable $x \sim \text{GIG}(\lambda, \chi, \psi)$ has probability density function $p(x) \propto x^{\lambda-1} \exp(-(\chi/x + \psi x)/2)$.

Similarly, we can get full conditionals of $(\beta_{2,1}^{(r)})^2$ under (3.8) and $(\beta_{3,1}^{(r)})^2$ under (3.9):

$$\left(\beta_{2,1}^{(r)}\right)^2 \mid \mathbf{B}_{2,(\cdot,r)}^{**}, \mathbf{B}_{3,(\cdot,r)}^{**} \sim \text{GIG}\left(\frac{M-P}{2}, \sum_{i_3=1}^P \left(\frac{\beta_{3,i_3}^{**(r)}}{\sigma_{3,i_3}^{(r)}}\right)^2, \sum_{i_2=2}^M \left(\frac{\beta_{2,i_2}^{**(r)}}{\sigma_{2,i_2}^{(r)}}\right)^2 + \left(\frac{1}{\sigma_{2,1}^{(r)}}\right)^2\right), \quad (3.11)$$

$$\left(\beta_{3,1}^{(r)}\right)^2 \mid \mathbf{B}_{3,(\cdot,r)}^{***}, \mathbf{B}_{1,(\cdot,r)}^{***} \sim \text{GIG}\left(\frac{P-M}{2}, \sum_{i_1=1}^M \left(\frac{\beta_{1,i_1}^{***(r)}}{\sigma_{1,i_1}^{(r)}}\right)^2, \sum_{i_3=2}^P \left(\frac{\beta_{3,i_3}^{***(r)}}{\sigma_{3,i_3}^{(r)}}\right)^2 + \left(\frac{1}{\sigma_{3,1}^{(r)}}\right)^2\right). \quad (3.12)$$

Algorithm 1 outlines how to interweave sampling under the base parameterization to the second one described in (3.4). Similar algorithms can be applied to the third and fourth parameterizations described in (3.6) and (3.7), incorporating with full conditionals in (3.11) and (3.12). Combining these three algorithms leads to a Gibbs sampler of which the full algorithm can be found in supplementary Appendix C.

Algorithm 1 Interweave between the base parameterization and the one in (3.4).

Step (a): Update $\mathbf{B}_1^{\text{old}}$ under the base parameterization.

Step (b): Store the first row of $\mathbf{B}_1^{\text{old}}$ into \mathbf{D}_1 and determine \mathbf{B}_1^* and \mathbf{B}_2^* .

Step (c): Sample $(\beta_{1,1}^{\text{new}(r)})^2$ for $r = 1, \dots, R$ using the corresponding full conditional in (3.10) and store sampled values into \mathbf{D}_1 .

Step (d): Update $\mathbf{B}_1^{\text{new}}$ and $\mathbf{B}_2^{\text{n\~{e}w}}$ with transformation $\mathbf{B}_1^{\text{new}} = \mathbf{B}_1^* \mathbf{D}_1$, $\mathbf{B}_2^{\text{n\~{e}w}} = \mathbf{B}_2^* \mathbf{D}_2^{-1}$.

If we only sample margins using Step (a), the algorithm is just a standard Gibbs sampler with the base parameterization. Every interweaving step starts at the base parameterization, then switches to an alternative parameterization and swaps back to the base one. Note that \mathbf{B}_2 's in this algorithm has superscript n\~{e}w. This is because \mathbf{B}_2 is included in two interweaving steps, but we only store one sample for \mathbf{B}_2 in each iteration. It will be easier to distinguish between the one stored (with superscript "new") and the one left (with superscript n\~{e}w). One can find the same superscripts in the full algorithm. Note that the interweaving strategy only improves the mixing of margins up to column permutation and sign switching, so we also proposed a post-processing procedure, inspired by the Match-Sign-Factor (MSF) algorithm in the R package **infinitefactor** (Poworoznek et al., 2021) to match columns and signs. More details about this procedure are in supplementary Appendix C.

3.2.3 Adaptive Inference of Rank

We aim to infer the rank by finding inactive columns in \mathbf{B} , i.e. those columns which do not contribute much to the tensor \mathcal{A} . An adaptive algorithm, inspired by Bhattacharya and Dunson (2011) and Legramanti et al. (2020), is displayed in Algorithm 2.

In this algorithm, R^* is the rank initialization set to be $\lceil 5 \log N \rceil$, which is the same as for the number of factors in Bhattacharya and Dunson (2011). Empirically, this initialization is large enough to estimate the coefficient matrix. In order to suffice diminishing adaptation condition (Roberts and

Rosenthal, 2007) for the weak law of large number in adaptive MCMC, we discard inactive columns in the m -th iteration with probability $p(m) = \exp(\alpha_0 + \alpha_1 m)$, where $\alpha_0 \leq 0$, $\alpha_1 < 0$. This is why we need to initialize α_0 and α_1 at the beginning of the algorithm. As $p(m)$ is getting smaller, R is less likely to change during the inference. Lastly, we need to set a criterion to decide whether a column in \mathbf{B} is active or not. In this paper, this criterion is related to the proportion of small magnitudes in $\mathcal{A}^{(r)}$, for $r = 1, \dots, R$. For ease of explanation, we omit m here. We regard an entry in $\mathcal{A}^{(r)}$ to have a small magnitude if its absolute value is smaller than a threshold γ_1 , e.g. $\gamma_1 = 10^{-3}$. If the proportion of small magnitudes in $\mathcal{A}^{(r)}$ is larger than another threshold γ_2 set *a-priori*, e.g. $\gamma_2 = 0.9$, then we regard the r -th column in \mathbf{B} as inactive. Note that this criterion is different from that in Fan et al. (2022), who treated a column as inactive if it has a l^2 norm close to a neighborhood of zero.

Adaptive inference begins after the \tilde{m} -th iteration to stabilize Markov chains and stops at the last iteration during the burn-in period to allow easy interpretation of margins. If the number of inactive columns is greater than 0, we remove these columns in \mathbf{B} and remove corresponding parameters in Φ , $\delta = (\delta_1, \dots, \delta_R)$, $\tau = (\tau_1, \dots, \tau_R)$. The rank will then be shrunk to a smaller number of active columns. If the algorithm does not detect any inactive column, we first sample a new column to Φ , a new entry to δ and subsequently compute the new entry in τ . A new column in \mathbf{B} will also be sampled using these newly-sampled hyperparameters.

Algorithm 2 Adaptive Inference of Rank

Initialize R^* , α_0 , α_1 and set a criterion

while iteration $\tilde{m} < m \leq m_{\text{burn-in}}$ **do**

Sample u from Uniform(0,1) and let $R^{(m)}$ be the rank at iteration m

if $p(m) \geq u$ **then**

$k = \#\{\text{inactive columns}\}$

if $k > 0$ **then**

Remove inactive columns in \mathbf{B} and related parameters

$R^{(m)} = R^{(m-1)} - k$

else

Add one column to \mathbf{B} and add values to related parameters

$$R^{(m)} = R^{(m-1)} + 1$$

4 Simulation Results

4.1 Data and Implementation

We assess the merits of inferring ranks using the MGP and the adaptive inferential scheme in 4.2, compared to the M-DGDP (Guhaniyogi et al., 2017) prior commonly used in tensor-structured models. Simulation results also show that the interweaving strategy can improve the mixing of margins in 4.3. We will leave the predictability comparison to the real data example. The following two subsections use the same simulation data, which includes three scenarios with different combinations of the number of time series and rank (N, R) : $(10, 3)$, $(20, 5)$ and $(50, 10)$. In each scenario, we generate 10 data sets following VAR(3) models with independently generated parameters. The coefficient matrix of each model is the 1-mode matricization of a tensor from a CP decomposition, and the covariance matrix is an identity matrix. Margins of the CP decomposition follow uniform distributions with different parameters; see Table 1 for more detail. All time series are then checked by Dickey-Fuller test and Kwiatkowski–Phillips–Schmidt–Shin (KPSS) tests for stationarity.

	(10,3)	(20,5)	(50,10)
B_1	U(-1,1)	U(-1,1)	U(-1,1)
B_2	U(-1,1)	U(-1,1)	U(-0.6,0.6)
$B_{3,(1,\cdot)}$	U(-1,1)	U(-1,1)	U(-0.6,0.6)
$B_{3,(2,\cdot)}$	U(-0.5,0.5)	U(-0.2,0.2)	U(-0.2,0.2)
$B_{3,(3,\cdot)}$	U(-0.1,0.1)	U(-0.1,0.1)	U(-0.1,0.1)

Table 1: Uniform distributions of margins in different locations indicated by rows and different combination of N and R indicated by columns.

We apply the MGP to both simulation experiments by setting $\nu = 3$, $\gamma_1 = 10^{-3}$, and $\gamma_2 = 0.9$. Apart from the MGP, we briefly introduce M-DGDP prior, which is a global-local shrinkage prior

proposed for tensor margins with the following expression:

$$\boldsymbol{\beta}_j^{(r)} \sim \mathcal{N}(\mathbf{0}, (\phi_r \tau) \mathbf{W}_{jr}), w_{jr,k} \sim \text{Exp}(\lambda_{jr}/2), \lambda_{jr} \sim \text{Gamma}(a_\lambda, b_\lambda),$$

$$\boldsymbol{\Phi} = (\phi_1, \dots, \phi_R)' \sim \text{Dirichlet}(\alpha, \dots, \alpha), \tau \sim \text{Gamma}(a_\tau, b_\tau),$$

where $\mathbf{W}_{jr} = \text{diag}(w_{jr,1}, \dots, w_{jr,I_j})$, $I_j = N$ when $j = 1, 2$ and $I_j = P$ when $j = 3$ in our case. α is uniformly distributed on a grid with values equally placed on $[R^{-3}, R^{-0.01}]$, and R is the rank set in advance. We follow the same setting of hyperparameters as in [Guhaniyogi et al. \(2017\)](#), i.e. $a_\lambda = 3$ and $b_\lambda = \sqrt[3]{a_\lambda}$, $a_\tau = R\alpha$, $b_\tau = \alpha \sqrt[3]{R}$.

For both priors, we set the rank as $\lceil 5 \log(N) \rceil$, but the adaptive inferential scheme is only applied when using the MGP after iteration reaches 200 in the burn-in period. For the M-DGDP, the rank is determined *a posteriori* by removing negligible margins as in [Algorithm 1](#). We implement all simulations with Intel(R) Xeon(R) Gold 6140 CPU 2.30GHzr and R 4.2.0.

4.2 Rank Selection

The first simulation assesses our approach to infer the rank R . Both samplers with MGP and M-DGDP were run for 10,000 iterations after 10,000 burn-in and incorporated the interweaving strategy. We record the performance of MGP and M-DGDP in [Table 2](#) including four evaluations: (1) mean squared error (MSE) of the coefficient matrix for coefficient accuracy; (2) averaged effective sample size (ESS) of coefficients for sampling efficiency; (3) averaged rank inferred (R) for rank accuracy; and (4) approximate running time for computational efficiency.

According to [Table 2](#), both models estimate coefficient matrices with similar accuracy under the MSE, with MGP results being slightly better than M-DGDP for all three scenarios. Ranks inferred by both priors are overestimated, but the MGP is able to infer ranks closer to the true ranks. The MGP also explores coefficient posteriors slightly more efficiently as suggested by ESS results from the first two scenarios. The adaptive shrinkage algorithm accelerates computation since the running time of the MGP grows more slowly with N and R in comparison to the growth rate of the M-DGDP.

This lead to a large difference if $N = 50$ and $R = 10$, when the inference with the MGP runs more than 10 times faster than the M-DGDP.

(N, R)	method	MSE	R	ESS	running time (hr)
(10,3)	MGP	0.054	4.8	4303.71	0.5
	M-DGDP	0.055	4.8	4000.62	1.1
(20, 5)	MGP	0.044	7.6	2532.11	0.8
	M-DGDP	0.046	9.3	2352.77	2.3
(50, 10)	MGP	0.044	11.1	918.13	1.1
	M-DGDP	0.045	15.3	929.69	13.4

Table 2: Performance of MGP and M-DGDP in 10 simulations for different dimensionality combinations.

4.3 Mixing

The second simulation focuses on the effect of the interweaving strategy. We choose three prior settings (standard normal, MGP, M-DGDP) to infer margins with/without interweaving. The burn-in period still has 10,000 iterations, but we change the number of iterations after burn-in to 100,000 to demonstrate results with longer chains. We conduct a column- and sign-switching method described in supplementary Appendix C to both samples with/without interweaving. This section focuses on the mixing of margins and one can find more details about the mixing of coefficients in Appendix D.

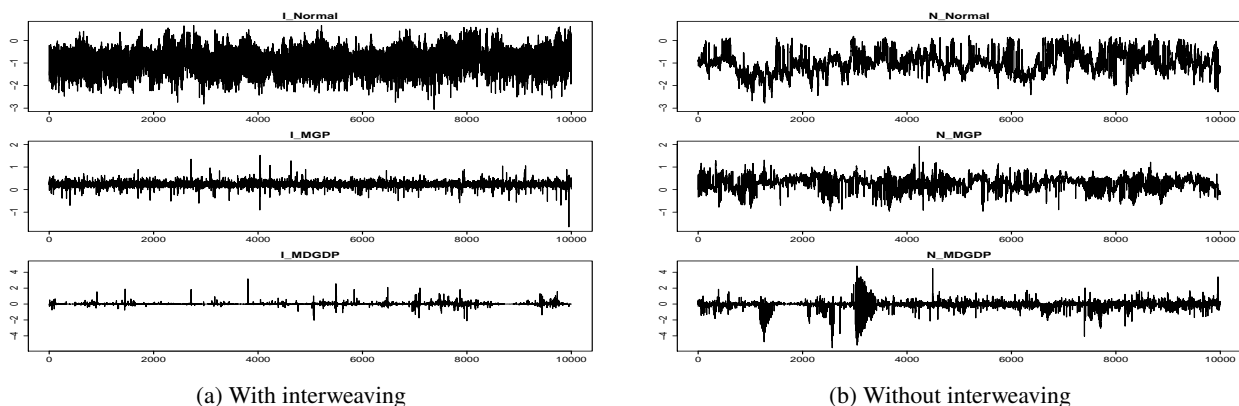


Figure 1: Trace plots of the first 10,000 draws of $\beta_{1,1}^{(1)}$ in $N = 10, R = 3$ scenario after burn-in period. The inferential scheme adopts standard normal (top), MGP (middle) and M-DGDP (bottom) as priors and applies with (left panel) and without (right panel) interweaving strategy.

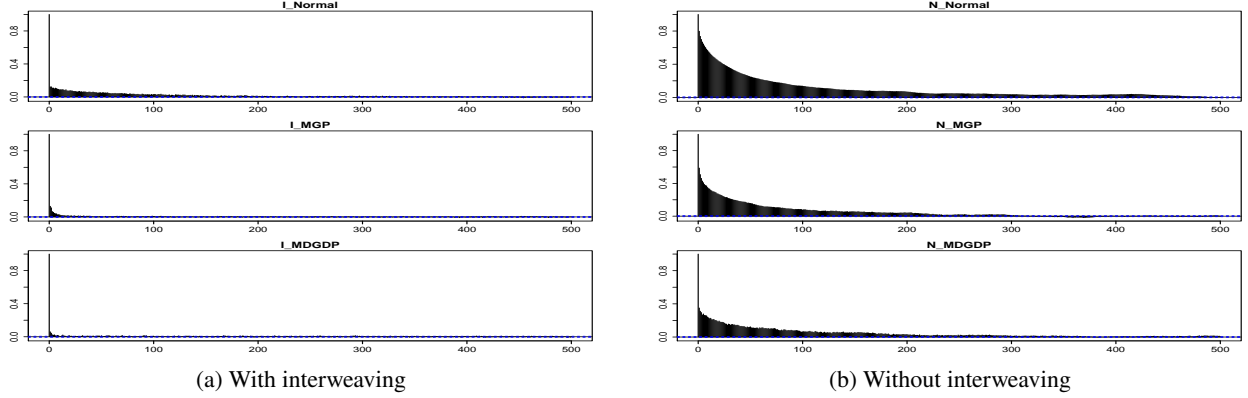


Figure 2: Autocorrelations of $\beta_{1,1}^{(1)}$ in $N = 10, R = 3$ scenario after the burn-in period. The inferential scheme adopts standard normal (top), MGP (middle) and M-DGDP (bottom) as priors and applies with (left panel) and without (right panel) interweaving strategy.

To give an insight into the effect of interweaving, Figure 1 shows trace plots of the margin $\beta_{1,1}^{(1)}$ when $N = 10$ and $R = 3$ based on different prior settings with/without interweaving. Even though we used the label- and sign-matching methods, trace plots without interweaving still suffer from the mixing problem, while the interweaving strategy substantially improves mixing. If we compare rows in Figure 1a, they present different behaviour about how the same inferential scheme explores posteriors using different prior settings. Draws inferred from the standard normal prior with interweaving jump between the maximum and minimum of a certain range frequently and do not have any extreme values. Whereas those inferred from MGP and M-DGDP with interweaving explore posteriors by staying around the mean with occasional jumps to some extreme values. MGP and M-DGDP also show the effect of shrinkage. Draws of M-DGDP without interweaving in Figure 1b also occasionally jump to extreme values, but these draws stay around these extreme values for several iterations, unlike its interweaving counterpart which returns immediately. Figure 2 displays autocorrelations (acfs) of all draws of $\beta_{1,1}^{(1)}$ after the burn-in period. These are consistent with the behaviour observed in Figure 1. The acfs from the interweaving strategy decay quickly, with only the one from the standard normal prior showing non-negligible values by 100 lags. All of these three acfs without interweaving remain large for many lags.

We follow the procedure in [Kastner et al. \(2017\)](#) to compute the inefficiency factor (IF) of each margin in different scenarios and prior settings. A smaller IF means that the sampling of a

parameter is more efficient. Figure 3 displays boxplots of IFs where each panel corresponds to a scenario with a combination of (N, R) and \mathbf{B}_j . Each data point in a boxplot is the averaged IF of a row in \mathbf{B}_j , for $j = 1, 2, 3$, inferred from one data set. Taking the Figure 3a as an example, there are 100 data points in each boxplot in the top two panels, since \mathbf{B}_1 and \mathbf{B}_2 have 10 rows for each of the 10 data sets; each boxplot in the bottom panel contains 30 data points because \mathbf{B}_3 have 3 rows. Similarly, the top two panels in Figure 3b and Figure 3c include boxplots with 200 and 500 points each, respectively; and each boxplot in the bottom panels in these two figures is composed of 30 data points. We use averaged IFs as data points because the numbers of averaged IFs in each boxplots in a panel are the same over different priors and algorithms, so these boxplots are more comparable than those using IFs directly. Moreover, using averaged IFs gives us better presentation since there are less outliers. Overall, averaged IFs with interweaving have lower median values and less variation, compared to their counterparts without interweaving. Although some of these boxplots corresponding to inference with interweaving have outliers, these outliers are lower than the upper whiskers of boxplots from the non-interwoven algorithm. While the number of outliers increases with N for both algorithms with/without interweaving, the median in each boxplot usually stays at the same level invariant to N .

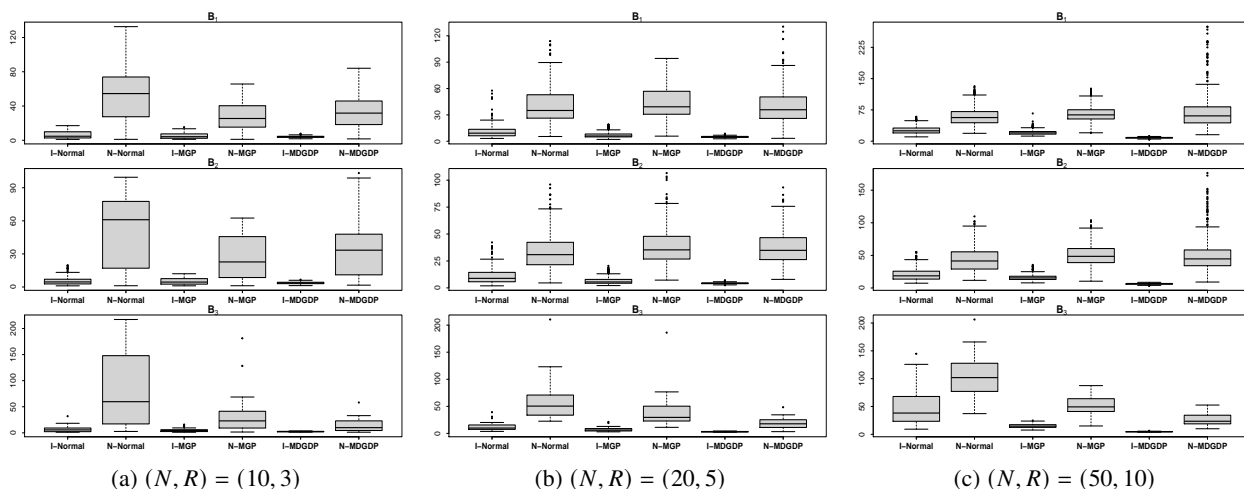


Figure 3: Boxplots of average inefficiency factor of \mathbf{B}_1 (top), \mathbf{B}_2 (middle) and \mathbf{B}_3 (bottom) from different scenarios: $(N, R) = (10, 3)$ (left), $(N, R) = (20, 5)$ (middle) and $(N, R) = (50, 10)$ (right). Inferential schemes with and without interweaving are represented as "I-" and "N-", respectively, followed by a prior setting.

5 Real Data Application

5.1 Data and Implementation

We use the US macroeconomic data described in [Korobilis and Pettenuzzo \(2019\)](#) to assess the utility of Tensor VARs. The data contains 124 quarterly variables from Federal Reserve Economic Data (FRED) ([McCracken and Ng, 2020](#)) and spans from 1959Q1 to 2015Q4. All time series are transformed to stationarity and standardized to have mean zero and variance one, to avoid any scaling issues. We extract 20 and 40 variables to construct medium-scale ($N=20$) and large-scale ($N=40$) data sets. The selected variables can be divided into 8 categories: (i) output and income, (ii) consumption, orders and inventories, (iii) labour market, (iv) prices, (v) interest rate, (vi) money and credit, (vii) stock market and (viii) exchange rate. Since we have a lower triangular matrix \mathbf{H} in the model, the order of time series matters. We follow [Carriero et al. \(2019\)](#) and [Bernanke et al. \(2005\)](#) by splitting time series to slow, fast groups and Federal Funds Rate (FEDFUNDS). The slow group contains variables that respond to a shock of FEDFUNDS with a lag, and variables in the fast group respond to it contemporaneously. The order is slow variables, FEDFUNDS, and fast variables. A full description of the variables selected and their transformations can be found in supplementary Appendix E.

For each data set, we estimate various VAR models with 5 lags. We consider both Tensor VARs with and without the additional own-lag matrix \mathbf{D} , denoted as Tensor MGP Own-Lag and Tensor MGP, respectively. For these two Tensor VARs, the threshold of small magnitude is 5×10^{-4} and its proportion threshold is 0.95. Implementation of the MGP is the same as in Section 4 and the prior for \mathbf{D} is described in Section 3.1.

For competitors, we include standard VARs with hierarchical Minnesota ([Giannone et al., 2015](#)), SSVS ([George et al., 2008](#)) and a specification of normal-gamma (NG) prior introduced to VARs by [Huber and Feldkircher \(2019\)](#). All of these three priors can be written as $A_{p,(i,j)} \sim \mathcal{N}\left(0, \underline{V}_{p,(i,j)}\right)$ for (i, j) entry in A_p , where $i, j = 1, \dots, N$ and $p = 1, \dots, 5$. For hierarchical Minnesota,

$$V_{-p,(i,j)} = \begin{cases} \frac{\lambda_1^2}{p^2}, & \text{if } i = j \\ \frac{\lambda_1^2 \lambda_2}{p^2} \frac{\hat{\sigma}_i}{\hat{\sigma}_j}, & \text{if } i \neq j \end{cases}, \text{ where } \hat{\sigma}_i^2 \text{ is the variance estimate of } \mathbf{y}_{t,i} \text{ sequence modelled by an}$$

AR(5) process. λ_1 and λ_2 have prior Gamma(0.01,0.01) and are inferred using a random walk Metropolis Hasting step. SSVS assigns either $\kappa_0^2 = 0.0001$ and $\kappa_1^2 = 4$ to $V_{-p,(i,j)}$ with a prior probability 0.5. We apply the NG described for \mathbf{H} and \mathbf{D} in Section 3.1 to the coefficient matrix. Priors for \mathbf{H} and stochastic volatility \mathbf{S}_t , for $t = 1, \dots, T$, are the same for all models. The MCMC sampler runs 10,000 iterations after the 10,000 burn-in period.

5.2 Forecasting Results

We follow the expanding window procedure to assess the forecasting performance of our models. Specifically, we first fit each VAR model with the historical data from 1959Q1 to 1984Q4, then get 1-, 2- and 4-step-ahead forecasts for 1985Q1, 1985Q2 and 1985Q4, respectively. Next, we expand the historical data with the endpoint at 1985Q1 and conduct the multi-step-ahead forecasting again. This procedure is repeated iteratively and stops after conducting the 1-step-ahead forecast of 2015Q4.

We use relative mean squared forecast error (RMSFE) and average log predictive likelihood (ALPL) to assess the point and density forecasting performance. We select 7 variables to evaluate the marginal forecasting performance of our models. These variables are Real Personal Income (RPI), CPI: All Items (CPIAUCSL), Real Gross Domestic Product (GDP), Federal Funds Rate (FEDFUNDS), Civilian Unemployment Rate (UNRATE), GDP deflator (GDPDEFL), 10-Year T-bond (GS10). For joint results, all 20 or 40 variables are considered. Marginal RMSFE for i -th variable from model m is defined as

$$\text{RMSFE}_{m,i} = \frac{\text{MSFE}_{m,i}}{\text{MSFE}_{\text{benchmark},i}}, \text{ with } \text{MSFE}_{m,i} = \frac{1}{\bar{T} - h - T + 1} \sum_{t=T}^{\bar{T}-h} (\mathbf{y}_{t+h,i} - \mathbb{E}(\mathbf{y}_{t+h,i} | \mathbf{y}_{1:t}, m))^2.$$

The benchmark model is a standard VAR with coefficients following a flat prior $\mathcal{N}(0, 10)$. \bar{T} is the total number of time points in the data set, and h is the horizon. $\mathbb{E}(\mathbf{y}_{t+h,i} | \mathbf{y}_{1:t}, m)$ is the Monte Carlo estimate of posterior predictive mean. The joint RMSFE for model m is formed with a similar

fraction of MSFE between model m and the benchmark model, but the joint MSFE of model m is

$$\text{MSFE}_{m,\text{joint}} = \frac{1}{(\bar{T} - h - T + 1)N} \sum_{n=1}^N \sum_{t=\bar{T}}^{\bar{T}-h} (\mathbf{y}_{t+h,i} - \mathbb{E}(\mathbf{y}_{t+h,i} | \mathbf{y}_{1:t}, m))^2.$$

The marginal ALPL for the i -th variable is

$$\text{ALPL}_i = \frac{1}{(\bar{T} - h - T + 1)} \sum_{t=\bar{T}}^{\bar{T}-h} \log p(\mathbf{y}_{t+h,i} | \mathbf{y}_{1:t}) = \frac{1}{(\bar{T} - h - T + 1)} \sum_{t=\bar{T}}^{\bar{T}-h} \text{LPDS}_{i,t+h}.$$

We follow [Billio et al. \(2022b\)](#) to compute $\text{LPDS}_{i,t+h}$ by randomly generating a sequence of stochastic volatility $\mathbf{s}_{t,i} = (s_{t+1,i}, \dots, s_{t+h,i})$ with parameters sampled in each iteration during inference. Then $\text{LPDS}_{i,t+h}$ is approximated by its Monte Carlo estimate,

$$\text{LPDS}_{i,t+h} = \log \int p(\mathbf{y}_{t+h,i} | \mathbf{y}_{1:t}, \mathbf{s}_{t,i}) p(\mathbf{s}_{t,i} | \mathbf{y}_{1:t}) d\mathbf{s}_{t,i} \approx \log \left(\frac{1}{L} \sum_{l=1}^L p(\mathbf{y}_{t+h,i} | \mathbf{y}_{1:t}, \mathbf{s}_{t,i}^{(l)}) \right).$$

Similarly, the joint ALPL is approximated by its Monte Carlo estimate in terms of stochastic volatility and the lower triangular matrix sampled in each iteration,

$$\text{ALPL}_{\text{joint}} \approx \frac{1}{(\bar{T} - h - T + 1)} \sum_{t=\bar{T}}^{\bar{T}-h} \log \left(\frac{1}{L} \sum_{l=1}^L p(\mathbf{y}_t | \mathbf{y}_{1:t}, \mathbf{S}_{(t+1):(t+h)}^{(l)}, \mathbf{H}^{(l)}) \right).$$

Table 3 and Table 4 show the performance of joint and marginal point forecasts inferred from data sets with different sizes. Overall, Tensor VARs achieve the best joint performance for most horizons in both cases. For the marginal performance of specific variables, Tensor VARs are better relative to standard VARs in 13 out of 21 cases for the medium data set and 17 out of 21 cases for the large data set. Forecasts of RPI, CPIAUCSL, GDPDEFL and GS10 are more favourable when using Tensor VARs, while standard VARs have better performance in forecasting GDP and UNRATE. For the two models considered in Tensor VARs, the performance of Tensor MGP and Tensor MGP Own-Lag is similar. If we move to individual models in standard VARs, the Minnesota prior achieves the best forecasting performance in GDP and UNRATE for all horizons when fitting the model with the medium-scale data. Forecasts of FEDFUNDS and UNRATE from SSVS prior are superior when the large-scale data is fitted to the model. Most RMSFEs decrease as the horizon gets longer, suggesting that the forecasting performance of flat prior deteriorates faster than other priors considered in this application. If we compare each evaluation in these two tables, most results inferred from the large

data set are smaller than those inferred from the medium data set. This is because of the more severe overfitting issue of the flat prior when considering more information in VARs.

Table 5 and Table 6 present density forecasting performance from the medium and large data sets. Note that the ALPL is not relative to the benchmark model because some ALPLs from the benchmark model have extremely small values (e.g. values smaller than -10^{-8}), so non-relative ALPL provides better presentation. Similar to the point forecast result, Tensor VARs get better performance when making joint density forecasts. They also outperform standard VARs in marginal cases since they are the best models in 17 out of 21 cases in both tables. We notice several differences between the performance evaluated by RMSFE and ALPL. Tensor MGP Own-Lag is more competitive in GDP density forecasts than point forecasts. The dominant model of forecasting GS10 changes from Tensor VARs to the standard VAR with NG prior if we switch the evaluation from RMSFE to ALPL. Although RMSFEs of joint forecasts from SSVS have similar scales as those from other models in Table 4, SSVS performs much worse than other models in the joint density forecasting as shown in Table 6.

Model	Horizon	RMSFE							
		Joint	RPI	CPIAUCSL	GDP	FEDFUNDS	UNRATE	GDPDEFL	GS10
Tensor MGP	1	0.634	0.536	0.839	0.564	0.367	0.532	0.639	0.639
	2	0.615	0.567	0.710	0.442	0.328	0.490	0.603	0.561
	4	0.531	0.412	0.796	0.487	0.283	0.435	0.560	0.578
Tensor MPG Own-Lag	1	0.617	0.548	0.816	0.546	0.345	0.514	0.569	0.634
	2	0.614	0.565	0.710	0.421	0.335	0.498	0.605	0.556
	4	0.531	0.412	0.796	0.467	0.284	0.449	0.566	0.576
Minnesota	1	0.625	0.576	0.817	0.503	0.357	0.486	0.576	0.651
	2	0.629	0.586	0.716	0.408	0.358	0.472	0.633	0.594
	4	0.546	0.425	0.794	0.462	0.298	0.433	0.590	0.626
SSVS	1	0.650	0.604	0.863	0.537	0.454	0.552	0.603	0.652
	2	0.647	0.608	0.746	0.469	0.445	0.554	0.628	0.587
	4	0.559	0.450	0.793	0.505	0.331	0.500	0.610	0.597
NG	1	0.647	0.554	0.851	0.607	0.364	0.589	0.627	0.635
	2	0.628	0.582	0.714	0.471	0.335	0.543	0.606	0.557
	4	0.537	0.420	0.795	0.499	0.281	0.458	0.565	0.576

Table 3: RMSFE of joint and marginal variables using the medium-scale data set. The best forecasts are in bold.

Model	Horizon	RMSFE							
		Joint	RPI	CPIAUCSL	GDP	FEDFUNDS	UNRATE	GDPDEFL	GS10
Tensor MGP	1	0.546	0.311	0.722	0.497	0.378	0.477	0.635	0.632
	2	0.461	0.221	0.526	0.460	0.256	0.475	0.433	0.537
	4	0.246	0.068	0.229	0.384	0.222	0.337	0.255	0.434
Tensor MPG Own-Lag	1	0.519	0.320	0.714	0.468	0.366	0.402	0.562	0.640
	2	0.457	0.221	0.528	0.439	0.265	0.448	0.435	0.539
	4	0.245	0.068	0.228	0.376	0.223	0.332	0.256	0.435
Minnesota	1	0.562	0.335	0.736	0.442	0.400	0.393	0.600	0.806
	2	0.526	0.232	0.536	0.439	0.326	0.439	0.463	0.750
	4	0.312	0.074	0.230	0.398	0.292	0.365	0.271	0.662
SSVS	1	0.518	0.382	0.724	0.466	0.313	0.387	0.602	0.634
	2	0.458	0.259	0.532	0.465	0.254	0.434	0.455	0.537
	4	0.247	0.086	0.229	0.392	0.220	0.332	0.259	0.437
NG	1	0.559	0.318	0.792	0.568	0.380	0.514	0.633	0.633
	2	0.466	0.225	0.534	0.511	0.266	0.493	0.433	0.537
	4	0.247	0.068	0.229	0.404	0.223	0.341	0.256	0.435

Table 4: RMSFE of joint and marginal variables using the large-scale data set. The best forecasts are in bold.

Model	Horizon	ALPL							
		Joint	RPI	CPIAUCSL	GDP	FEDFUNDS	UNRATE	GDPDEFL	GS10
tensor MGP	1	-18.760	-1.206	-1.205	-0.998	-0.418	-0.926	-1.160	-1.310
	2	-19.899	-1.257	-1.374	-1.057	-0.519	-1.027	-1.192	-1.309
	4	-20.892	-1.302	-1.404	-1.141	-0.612	-1.138	-1.182	-1.296
Tensor MPG Own-Lag	1	-17.921	-1.213	-1.160	-0.964	-0.311	-0.913	-1.056	-1.305
	2	-19.690	-1.253	-1.369	-1.009	-0.490	-1.042	-1.179	-1.298
	4	-21.136	-1.304	-1.398	-1.097	-0.576	-1.185	-1.166	-1.288
Minnesota	1	-18.683	-1.260	-1.177	-0.946	-0.440	-0.897	-1.078	-1.307
	2	-20.263	-1.286	-1.372	-1.015	-0.621	-1.002	-1.216	-1.347
	4	-21.542	-1.343	-1.405	-1.113	-0.695	-1.140	-1.227	-1.344
SSVS	1	-18.427	-1.233	-1.190	-0.967	-0.332	-0.891	-1.120	-1.306
	2	-20.098	-1.267	-1.376	-1.051	-0.534	-1.033	-1.224	-1.309
	4	-21.391	-1.312	-1.395	-1.128	-0.623	-1.176	-1.213	-1.291
NG	1	-19.556	-1.228	-1.237	-1.039	-0.461	-0.998	-1.142	-1.292
	2	-20.580	-1.282	-1.373	-1.090	-0.590	-1.096	-1.195	-1.294
	4	-21.696	-1.329	-1.391	-1.154	-0.641	-1.199	-1.190	-1.284

Table 5: ALPL of joint and marginal variables using the medium-scale data set. The best forecasts are in bold.

5.3 Interpretation

Since Tensor MGP Own-Lag achieves better joint performance, we demonstrate how to interpret Tensor VARs by fitting it with the whole large-scale data set ($N=40$). The model infers the rank as 3 (see Figure 5), which means this Tensor VAR structure reduces the number of parameters in the coefficient matrix from 8,000 (standard VAR(5)) to 455. Implemented with the same processor mentioned in Section 4, the runtime of Tensor MGP Own-Lag is around 2.9 hours, compared to 11 hours by using a standard VAR with the NG.

Model	Horizon	ALPL							
		Joint	RPI	CPIAUCSL	GDP	FEDFUNDS	UNRATE	GDPDEFLL	GS10
tensor MGP	1	-36.809	-1.195	-1.183	-1.022	-0.370	-0.995	-1.172	-1.310
	2	-39.325	-1.263	-1.348	-1.060	-0.474	-1.083	-1.187	-1.300
	4	-41.590	-1.303	-1.369	-1.132	-0.576	-1.189	-1.187	-1.290
tensor MPG Own-Lag	1	-34.596	-1.224	-1.153	-0.971	-0.300	-0.899	-1.063	-1.323
	2	-38.578	-1.271	-1.373	-1.022	-0.480	-1.027	-1.174	-1.304
	4	-40.949	-1.314	-1.392	-1.113	-0.561	-1.167	-1.166	-1.292
Minnesota	1	-39.416	-1.254	-1.176	-0.984	-0.487	-0.919	-1.126	-1.482
	2	-42.514	-1.289	-1.385	-1.065	-0.697	-1.002	-1.238	-1.525
	4	-45.142	-1.341	-1.421	-1.162	-0.805	-1.153	-1.262	-1.587
SSVS	1	-66.780	-26.497	-1.186	-1.022	-0.242	-0.877	-1.230	-1.311
	2	-55.001	-2.355	-1.365	-1.097	-0.497	-1.001	-1.306	-1.304
	4	-58.560	-7.303	-1.388	-1.194	-0.592	-1.149	-1.309	-1.297
NG	1	-39.760	-1.224	-1.272	-1.094	-0.438	-1.056	-1.169	-1.309
	2	-41.137	-1.274	-1.354	-1.134	-0.554	-1.107	-1.187	-1.300
	4	-42.318	-1.318	-1.364	-1.183	-0.621	-1.192	-1.187	-1.290

Table 6: ALPL of joint and marginal variables using the large-scale data set. The best forecasts are in bold.

According to (2.5), a Tensor VAR can be interpreted as a factor model with observable factors and loadings with different effects. We firstly focus on these factors by recording their evolution over time. As presented in Figure 4, factors are consistent with recession periods indicated by the National Bureau of Economic Research (NBER) (available on <https://fred.stlouisfed.org/series/USRECQ>). The first factor peaks during the recession of 1969–1970, the stagflation in the 1970s, the 1979 energy crisis, the early 1990s recession, the dot-com bubble in the early 2000s and the financial crisis of 2008. Although the median of the second factor is flat, it is more uncertain during the above recession periods. The "double-dip" recession in 1980 is highlighted by the more volatile behaviour in the third factor. It is unsurprising for this consistency because these factors are linear functions of lagged data.

Next, we interpret the model by looking at different loadings. Figure 5 depicts the posterior mean of response, predictor and temporal loadings with important margins highlighted. These loadings reflect the increasing shrinkage property of the MGP because the first column in each loading is the densest. Highlighted margins in these columns show that the first factor conveys the general economic impact in the previous quarter on output and income category, because the first column of the response loading features larger magnitudes for margins in this category, and only the margin of the first lag in the temporal loading is highlighted. While the second columns

are less informative, the third ones suggest that the corresponding factor mainly describes the interrelationships within the interest rate category. Note that these loadings and factors focus on exploring the cross-lag effects, while the inferred own-lag matrix D in supplementary Appendix D provides more information about the own-lag effects.

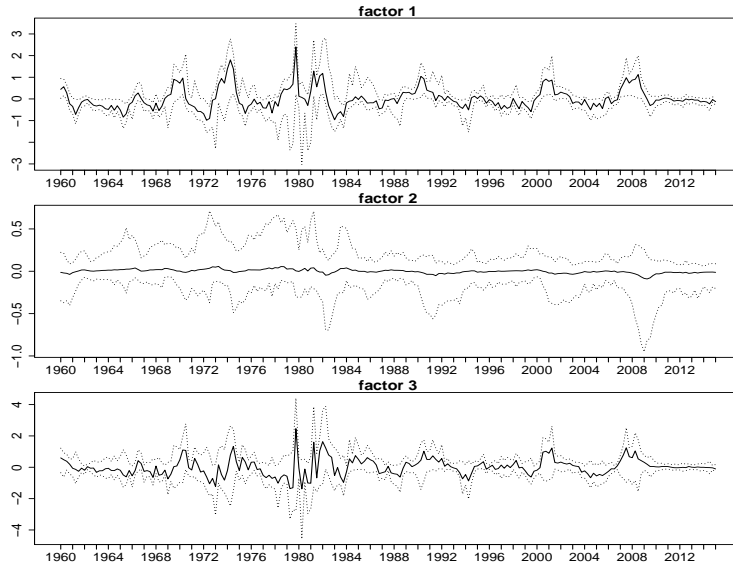


Figure 4: Time series plots of factors with median (solid line) and 80% credible interval (dashed line). The model includes an own-lag matrix.

5.4 Effect of D

This subsection gives evidence that D can separate the own-lag and cross-lag effects, and allow the inference of ranks to be stable. We use Tensor MGP (without D) to conduct the same experience as in Section 5.3. As depicted in Figure 6, the three loadings are denser than those inferred from the Tensor MGP Own-Lag, and important margins have larger magnitudes because Tensor MGP needs to explore both the own-lag and cross-lag effects without the help of D . Among important margins in the first columns of response and predictor loadings, margins for PAYEMS have magnitudes much larger than those of other margins, so the first factor is mainly driven by the own-lag effect of PAYEMS. Similarly, the second factor is primarily contributed from the own-lag effect of M2REAL. To sum up, it is easier to detect the own-lag effects from loadings inferred by Tensor MGP than by

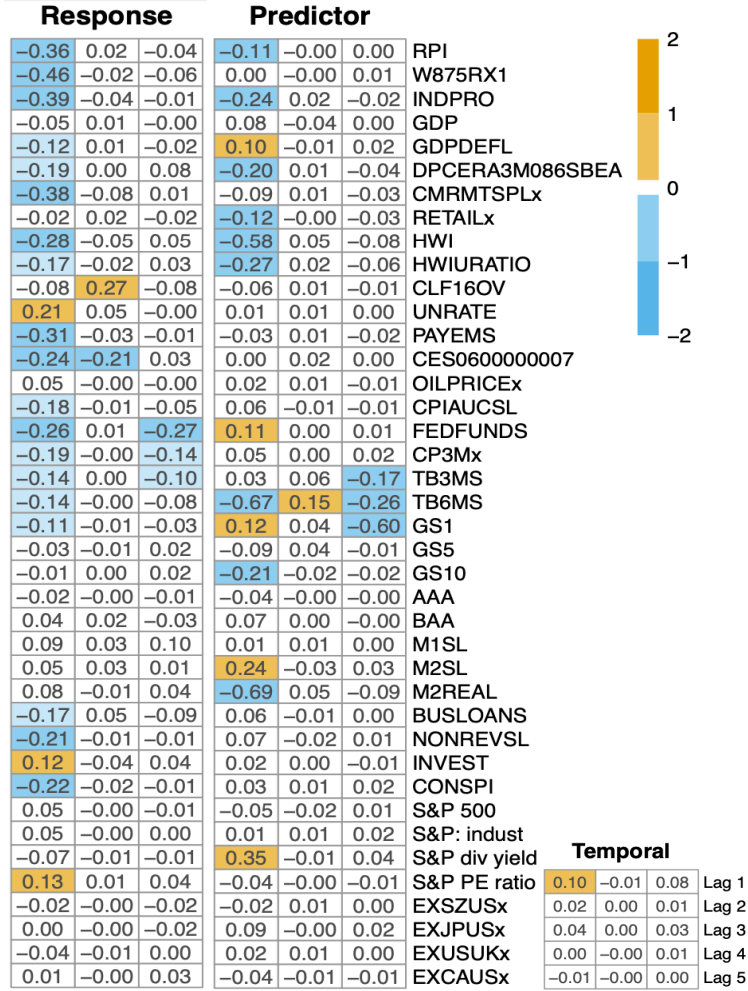


Figure 5: Posterior mean of response, predictor and temporal loadings inferred from Tensor MGP Own-Lag. Important margins have magnitudes greater than 0.1.

Tensor MGP Own-Lag, suggesting that the additional own-lag matrix in the latter model allows the tensor to explore more cross-lag effects.

The ranks inferred using Tensor MGP Own-Lag and Tensor MGP are the same in this experience, but it is unclear how the inferential results of ranks differ if we fit these two models to more data sets. To understand this, we use the expanding window procedure in Section 5.2 to obtain time series plots of ranks inferred from these two Tensor VARs as shown in Figure 7. The x-axis indicates the last time point used when fitting the model. Tensor MGP Own-Lag infers most of the ranks to be 3 or 4, except in one case when the inferred rank is 5. In contrast, Tensor MGP starts by inferring ranks like results from Tensor MGP Own-Lag, but ranks jump to larger values after the data set spans to

1996. One possible reason of this finding is that Tensor MGP needs generally more columns in loadings to model the data as we include more data points, whereas Tensor MGP Own-Lag can adjust D to stabilize the inference of the rank.

6 Conclusion

In this paper, we propose in- and post-processing algorithms to infer ranks of Tensor VARs and alleviate the mixing issue of margins. In particular, we applied the Multiplicative Gamma Prior (MGP) to margins and use an adaptive inferential scheme to infer the rank. To overcome the mixing issue, we introduce an interweaving Gibbs sampler to allow better mixing of Markov chains and match labels and signs after the inference. In the simulation experiment, Tensor VARs with the MGP can infer ranks more accurately and efficiently than models with M-DGDP. The interweaving Gibbs sampler improves mixing evaluated by inefficiency factors, and we demonstrate the necessity of label and sign matching by trace plots of margins.

In the real data application, we conduct multi-step-ahead forecasting and interpret results from Tensor VARs with and without the own-lag matrix. Tensor VARs achieve the best joint performance in point and density forecasting, and they are competitive to standard VARs with a range of prior choices in marginal forecasting. Apart from forecasting performance, Tensor VARs can effectively reduce the number of parameters and speed up the inference. We interpret Tensor VARs as factor models with observable factors explaining the economic dynamic. The additional own-lag matrix induces the tensor part to focus on the cross-lag effects.

Several extensions can be investigated in the future. Firstly, the model structure of a Tensor VAR is not static as shown in Figure 7b, so it will be interesting to adopt time-varying margins and rank to the Tensor VAR. A related work is studied by [Zhang et al. \(2021\)](#), who kept margins time-invariant and switched each column of the tensor matrix B on or off with a prior. Secondly, we can modify the MGP to include a local parameter corresponding to each row of the loadings so as to provide more interpretability. Lastly, a similar MCMC scheme can be applied to Tucker

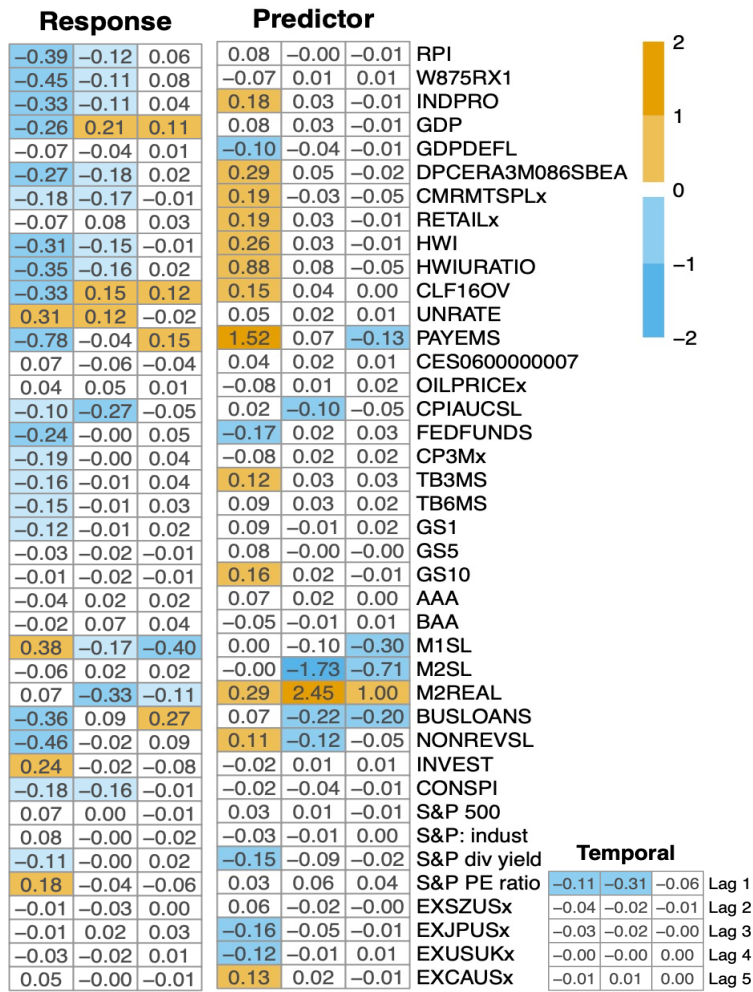


Figure 6: Posterior mean of response, predictor and temporal loadings inferred from Tensor MGP. Important margins have magnitudes greater than 0.1.

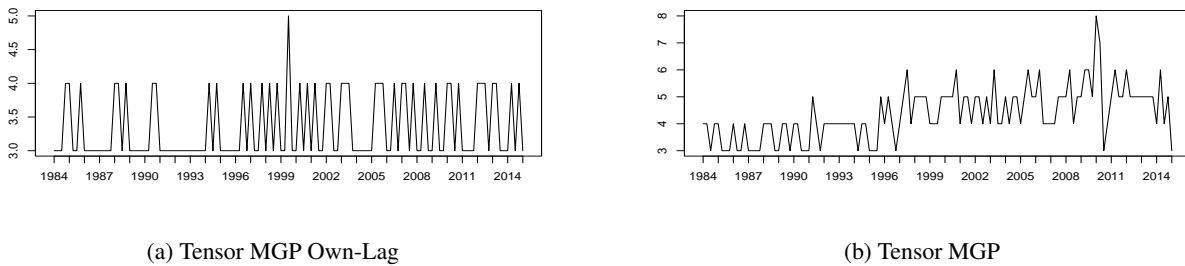


Figure 7: Time series plots of rank inferred by Tensor MGP Own-Lag and Tensor MGP.

decomposition ([Tucker, 1966](#)), another popular tensor decomposition with a more flexible structure comparing to the CP decomposition.

References

- Bañbura, M., Giannone, D., and Reichlin, L. (2010). Large Bayesian vector auto regressions. *Journal of Applied Econometrics*, 25(1):71–92.
- Bernanke, B. S., Boivin, J., and Eliasch, P. (2005). Measuring the effects of monetary policy: a factor-augmented vector autoregressive (FAVAR) approach. *The Quarterly Journal of Economics*, 120(1):387–422.
- Bhattacharya, A. and Dunson, D. B. (2011). Sparse Bayesian infinite factor models. *Biometrika*, 98(2):291–306.
- Billio, M., Casarin, R., and Iacopini, M. (2022a). Bayesian markov-switching tensor regression for time-varying networks. *Journal of the American Statistical Association*, pages 1–13.
- Billio, M., Casarin, R., Iacopini, M., and Kaufmann, S. (2022b). Bayesian dynamic tensor regression. *Journal of Business & Economic Statistics*. to appear.
- Brown, P. J. and Griffin, J. E. (2010). Inference with normal-gamma prior distributions in regression problems. *Bayesian Analysis*, 5(1):171–188.
- Carriero, A., Chan, J., Clark, T. E., and Marcellino, M. (2022). Corrigendum to “Large Bayesian vector autoregressions with stochastic volatility and non-conjugate priors”[*J. econometrics* 212(1)(2019) 137–154]. *Journal of Econometrics*, 227(2):506–512.
- Carriero, A., Clark, T. E., and Marcellino, M. (2019). Large Bayesian vector autoregressions with stochastic volatility and non-conjugate priors. *Journal of Econometrics*, 212(1):137–154.
- Carriero, A., Kapetanios, G., and Marcellino, M. (2011). Forecasting large datasets with bayesian reduced rank multivariate models. *Journal of Applied Econometrics*, 26(5):735–761.
- Chen, R., Yang, D., and Zhang, C.-H. (2022). Factor models for high-dimensional tensor time series. *Journal of the American Statistical Association*, 117(537):94–116.
- Cogley, T. and Sargent, T. J. (2005). Drifts and volatilities: monetary policies and outcomes in the post WWII US. *Review of Economic Dynamics*, 8(2):262–302.

- Doan, T., Litterman, R., and Sims, C. (1984). Forecasting and conditional projection using realistic prior distributions. *Econometric Reviews*, 3(1):1–100.
- Durante, D. (2017). A note on the multiplicative gamma process. *Statistics & Probability Letters*, 122:198–204.
- Fan, J., Sitek, K., Chandrasekaran, B., and Sarkar, A. (2022). Bayesian tensor factorized mixed effects vector autoregressive processes for inferring Granger causality patterns from high-dimensional neuroimage data. *arXiv preprint arXiv:2206.10757*.
- Follett, L. and Yu, C. (2019). Achieving parsimony in Bayesian vector autoregressions with the horseshoe prior. *Econometrics and Statistics*, 11:130–144.
- George, E. I., Sun, D., and Ni, S. (2008). Bayesian stochastic search for VAR model restrictions. *Journal of Econometrics*, 142(1):553–580.
- Giannone, D., Lenza, M., and Primiceri, G. E. (2015). Prior selection for vector autoregressions. *Review of Economics and Statistics*, 97(2):436–451.
- Giannone, D., Lenza, M., and Primiceri, G. E. (2021). Economic predictions with big data: The illusion of sparsity. *Econometrica*, 89(5):2409–2437.
- Gruber, L. and Kastner, G. (2022). Forecasting macroeconomic data with Bayesian VARs: Sparse or dense? it depends! *arXiv preprint arXiv:2206.04902*.
- Guhaniyogi, R., Qamar, S., and Dunson, D. B. (2017). Bayesian tensor regression. *The Journal of Machine Learning Research*, 18(1):2733–2763.
- Guhaniyogi, R. and Spencer, D. (2021). Bayesian tensor response regression with an application to brain activation studies. *Bayesian Analysis*, 16(4):1221–1249.
- Hsu, N.-J., Hung, H.-L., and Chang, Y.-M. (2008). Subset selection for vector autoregressive processes using lasso. *Computational Statistics & Data Analysis*, 52(7):3645–3657.
- Huber, F. and Feldkircher, M. (2019). Adaptive shrinkage in Bayesian vector autoregressive models. *Journal of Business & Economic Statistics*, 37(1):27–39.

- Huber, F., Kastner, G., and Feldkircher, M. (2019). Should I stay or should I go? A latent threshold approach to large-scale mixture innovation models. *Journal of Applied Econometrics*, 34(5):621–640.
- Jacquier, E., Polson, N. G., and Rossi, P. E. (2002). Bayesian analysis of stochastic volatility models. *Journal of Business & Economic Statistics*, 20(1):69–87.
- Kastner, G. (2016). Dealing with stochastic volatility in time series using the r package stochvol. *Journal of Statistical Software*, 69(5):1–30.
- Kastner, G. and Frühwirth-Schnatter, S. (2014). Ancillarity-sufficiency interweaving strategy (ASIS) for boosting MCMC estimation of stochastic volatility models. *Computational Statistics & Data Analysis*, 76:408–423.
- Kastner, G., Frühwirth-Schnatter, S., and Lopes, H. F. (2017). Efficient Bayesian inference for multivariate factor stochastic volatility models. *Journal of Computational and Graphical Statistics*, 26(4):905–917.
- Kiers, H. A. (2000). Towards a standardized notation and terminology in multiway analysis. *Journal of Chemometrics: A Journal of the Chemometrics Society*, 14(3):105–122.
- Kim, S., Shephard, N., and Chib, S. (1998). Stochastic volatility: likelihood inference and comparison with ARCH models. *The Review of Economic Studies*, 65(3):361–393.
- Kolda, T. G. and Bader, B. W. (2009). Tensor decompositions and applications. *SIAM Review*, 51(3):455–500.
- Korobilis, D. and Pettenuzzo, D. (2019). Adaptive hierarchical priors for high-dimensional vector autoregressions. *Journal of Econometrics*, 212(1):241–271.
- Legramanti, S., Durante, D., and Dunson, D. B. (2020). Bayesian cumulative shrinkage for infinite factorizations. *Biometrika*, 107(3):745–752.
- Litterman, R. B. (1986). Forecasting with Bayesian vector autoregressions—five years of experience. *Journal of Business & Economic Statistics*, 4(1):25–38.

- Litterman, R. B. et al. (1979). Techniques of forecasting using vector autoregressions. Working Paper 115, Federal Reserve Bank of Minneapolis.
- McCracken, M. and Ng, S. (2020). FRED-QD: A quarterly database for macroeconomic research. Working paper, National Bureau of Economic Research.
- Ng, S. (2013). Variable selection in predictive regressions. *Handbook of economic forecasting*, 2:752–789.
- Nicholson, W. B., Wilms, I., Bien, J., and Matteson, D. S. (2020). High Dimensional Forecasting via Interpretable Vector Autoregression. *Journal of Machine Learning Research*, 21(166):1–52.
- Poworoznek, E., Ferrari, F., and Dunson, D. (2021). Efficiently resolving rotational ambiguity in Bayesian matrix sampling with matching. *arXiv preprint arXiv:2107.13783*.
- Roberts, G. O. and Rosenthal, J. S. (2007). Coupling and ergodicity of adaptive Markov chain Monte Carlo algorithms. *Journal of Applied Probability*, 44(2):458–475.
- Rousseau, J. and Mengersen, K. (2011). Asymptotic behaviour of the posterior distribution in overfitted mixture models. *Journal of the Royal Statistical Society: Series B (Statistical Methodology)*, 73(5):689–710.
- Shojaie, A. and Michailidis, G. (2010). Discovering graphical Granger causality using the truncating lasso penalty. *Bioinformatics*, 26(18):i517–i523.
- Simpson, M. (2015). Application of interweaving in DLMS to an exchange and specialization experiment. In *Bayesian Statistics from Methods to Models and Applications*, pages 75–90. Springer.
- Simpson, M., Niemi, J., and Roy, V. (2017). Interweaving Markov chain Monte Carlo strategies for efficient estimation of dynamic linear models. *Journal of Computational and Graphical Statistics*, 26(1):152–159.
- Sims, C. A. (1980). Macroeconomics and reality. *Econometrica*, 1–48.
- Song, S. and Bickel, P. J. (2011). Large vector auto regressions. *arXiv preprint arXiv:1106.3915*.
- Stock, J. H. and Watson, M. (2011). Dynamic factor models. *Oxford Handbooks Online*.

- Stock, J. H. and Watson, M. W. (2005). Implications of dynamic factor models for VAR analysis.
- Tibshirani, R. (1996). Regression shrinkage and selection via the lasso. *Journal of the Royal Statistical Society: Series B (Methodological)*, 58(1):267–288.
- Tucker, L. R. (1966). Some mathematical notes on three-mode factor analysis. *Psychometrika*, 31(3):279–311.
- Velu, R. P., Reinsel, G. C., and Wichern, D. W. (1986). Reduced rank models for multiple time series. *Biometrika*, 73(1):105–118.
- Wang, D., Zheng, Y., Lian, H., and Li, G. (2021). High-dimensional vector autoregressive time series modeling via tensor decomposition. *Journal of the American Statistical Association*, 1–19.
- Yu, Y. and Meng, X.-L. (2011). To center or not to center: That is not the question—an Ancillarity–Sufficiency Interweaving Strategy (ASIS) for boosting MCMC efficiency. *Journal of Computational and Graphical Statistics*, 20(3):531–570.
- Zhang, W., Cribben, I., Guindani, M., et al. (2021). Bayesian time-varying tensor vector autoregressive models for dynamic effective connectivity. *arXiv preprint arXiv:2106.14083*.
- Zhou, H., Li, L., and Zhu, H. (2013). Tensor regression with applications in neuroimaging data analysis. *Journal of the American Statistical Association*, 108(502):540–552.

A Basic Notations and Operations

We follow the convention in tensor literature to introduce some basic notations and operations. See [Kolda and Bader \(2009\)](#) for a review. A tensor \mathcal{A} is a J th-order tensor if $\mathcal{A} \in \mathbb{R}^{I_1 \times \dots \times I_J}$ with entries $\mathcal{A}_{i_1, \dots, i_J}$ for $i_j = 1, \dots, I_j$. first- and second-order tensors are simply vectors and matrices. Similar to the definition of a diagonal matrix, a tensor is called a J th-order *superdiagonal* tensor if $I_1 = \dots = I_J = I$ and only its (i, \dots, i) entries are non-zero for $i = 1, \dots, I$. Extracting entries by a selected index from a matrix \mathbf{A} and a tensor \mathcal{A} is akin. We denote $\mathbf{A}_{(i_1, \cdot)}$, $\mathbf{A}_{(\cdot, i_2)}$ and $\mathcal{A}_{(\dots, i_j, \dots)}$ as the i_1 -th row, the i_2 -th column in \mathbf{A} and a $(J - 1)$ th-order tensor with entries having the index i_j on the j -th dimension in \mathcal{A} .

Matricization of a J th-order tensor ($J > 2$) is an operation that transforms the tensor into a matrix. There are J possible matricizations for a J th-order tensor \mathcal{A} , and the matricization to the j -th dimension is called the *mode- j matricization* with notation $\mathcal{A}_{(j)} \in \mathbb{R}^{I_j \times \prod_{j' \neq j} I_{j'}}$, where the i_j -th row corresponds to the vectorization of $\mathcal{A}_{(\dots, i_j, \dots)}$. The *j -mode product* of \mathcal{A} and a matrix $\mathbf{B} \in \mathbb{R}^{K \times I_j}$ is denoted as $\mathcal{A} \times_j \mathbf{B}$, which gives a J th-order tensor $\mathbf{C} \in \mathbb{R}^{I_1 \times \dots \times I_{j-1} \times K \times I_{j+1} \times \dots \times I_J}$ with the $(i_1, \dots, i_{j-1}, k, i_{j+1}, \dots, i_J)$ entry as

$$\mathbf{C}_{i_1, \dots, i_{j-1}, k, i_{j+1}, \dots, i_J} = \sum_{i_j=1}^{I_j} \mathcal{A}_{i_1, \dots, i_j, \dots, i_J} \mathbf{B}_{k, i_j}.$$

The following are some preliminaries for tensor decompositions. The vector outer product of two vectors $\boldsymbol{\beta}_1 \in \mathbb{R}^{I_1}$ and $\boldsymbol{\beta}_2 \in \mathbb{R}^{I_2}$ is $\boldsymbol{\beta}_1 \circ \boldsymbol{\beta}_2$, yielding an I_1 -by- I_2 matrix with its (i_1, i_2) entry as $\beta_{1, i_1} \beta_{2, i_2}$. Assume we have J vectors with $\boldsymbol{\beta}_j \in \mathbb{R}^{I_j}$ denoting the j -th vector, then the *J -way outer product* of these vectors, $\boldsymbol{\beta}_1 \circ \dots \circ \boldsymbol{\beta}_J$, is a $I_1 \times \dots \times I_J$ tensor, with (i_1, \dots, i_J) entry as $\beta_{1, i_1} \dots \beta_{J, i_J}$.

The most prominent tensor decompositions are CANDECOMP/PARAFAC (CP) decomposition (Kiers, 2000) and Tucker decomposition (Tucker, 1966). A rank- R CP decomposition of a J th-order tensor is

$$\mathcal{A} = \sum_{r=1}^R \boldsymbol{\beta}_1^{(r)} \circ \dots \circ \boldsymbol{\beta}_J^{(r)} = \sum_{r=1}^R \mathcal{A}^{(r)}, \quad (\text{A.1})$$

where entries in $\boldsymbol{\beta}_j^{(r)} \in \mathbb{R}^{I_j}$ for $j = 1, \dots, J$ and $r = 1, \dots, R$, are *margins* of the tensor, $\mathcal{A}^{(r)} = \boldsymbol{\beta}_1^{(r)} \circ \dots \circ \boldsymbol{\beta}_J^{(r)} \in \mathbb{R}^{I_1 \times \dots \times I_J}$.

Instead of having only one rank, Tucker decomposition has J ranks, R_1, \dots, R_J , to decompose a J th-order tensor as

$$\mathcal{A} = \sum_{r_1=1}^{R_1} \sum_{r_2=1}^{R_2} \dots \sum_{r_J=1}^{R_J} \mathcal{G}_{r_1, \dots, r_J} \boldsymbol{\beta}_1^{(r_1)} \circ \dots \circ \boldsymbol{\beta}_J^{(r_J)}, \quad (\text{A.2})$$

where \mathcal{G} is a J th-order tensor with dimension $R_1 \times \dots \times R_J$. Tucker decomposition is the generalization of the CP decomposition because they are equivalent when \mathcal{G} is a superdiagonal tensor.

B Full Conditionals and Derivations

B.1 Full Conditionals of B_1, B_2, B_3 and D

In this subsection, we consider a Tensor VAR with the additional own-lag matrix D . The inference of a Tensor VAR without D is simply to treat D as a zero matrix. Recall a Tensor VAR in terms of B_1, B_2 and B_3 :

$$\mathbf{y}_t^* = \left(\mathbf{x}_t' (\mathbf{B}_3 \otimes \mathbf{B}_2) \mathcal{I}'_{(1)} \otimes \mathbf{I}_N \right) \text{vec}(\mathbf{B}_1) + \boldsymbol{\epsilon}_t \quad (\text{B.1})$$

$$= \mathbf{B}_1 \mathcal{I}_{(1)} \left((\mathbf{B}_3' \mathbf{X}_t') \otimes \mathbf{I}_R \right) \text{vec}(\mathbf{B}_2') + \boldsymbol{\epsilon}_t \quad (\text{B.2})$$

$$= \mathbf{B}_1 \mathcal{I}_{(1)} \left(\mathbf{I}_R \otimes (\mathbf{B}_2' \mathbf{X}_t') \right) \text{vec}(\mathbf{B}_3) + \boldsymbol{\epsilon}_t. \quad (\text{B.3})$$

We assume the terms before vectorizations of B_1, B_2' and B_3 as $\mathbf{Z}_{t,1}, \mathbf{Z}_{t,2}$ and $\mathbf{Z}_{t,3}$, respectively. Given other parameters, the full conditional of $\text{vec}(\mathbf{B}_j)$ for $j = 1, 3$ or that of $\text{vec}(\mathbf{B}'_j)$ for $j = 2$ is $\mathcal{N}(\bar{\boldsymbol{\mu}}_j, \bar{\boldsymbol{\Sigma}}_j)$ with

$$\begin{aligned} \bar{\boldsymbol{\Sigma}}_j^{-1} &= \underline{\boldsymbol{\Sigma}}_j^{-1} + \sum_{t=1}^T \mathbf{Z}'_{t,j} \mathbf{H}' \mathbf{S}_t^{-1} \mathbf{H} \mathbf{Z}_{t,j}, \\ \bar{\boldsymbol{\mu}}_j &= \bar{\boldsymbol{\Sigma}}_j^{-1} \sum_{t=1}^T \mathbf{Z}'_{t,j} \mathbf{H}' \mathbf{S}_t^{-1} \tilde{\mathbf{y}}_t^*, \end{aligned}$$

where $\tilde{\mathbf{y}}_t^* = \mathbf{H} \mathbf{y}_t^* = \mathbf{H}(\mathbf{y}_t - \mathbf{D} \mathbf{x}_t)$, $\underline{\boldsymbol{\Sigma}}_j$ is the prior covariance matrix of the corresponding vector.

Given B_1, B_2, B_3 and other parameters, we can infer D in a similar way as [Carriero et al. \(2022\)](#). Assume that $\mathbf{D} = (\text{diag}(d_{1,1}, \dots, d_{N,1}), \dots, \text{diag}(d_{1,P}, \dots, d_{N,P}))$, and $\mathbf{y}_t^{**} = \mathbf{y}_t - \mathcal{A}_{(1)} \mathbf{x}_t = \mathbf{D} \mathbf{x}_t + \boldsymbol{\epsilon}_t$, if we multiply both sides of the equation aforementioned with \mathbf{H} , we get $\tilde{\mathbf{y}}_t^{**} = \mathbf{H} \mathbf{y}_t^{**} = \mathbf{H} \mathbf{D} \mathbf{x}_t + \mathbf{u}_t$, where $\mathbf{u}_t \sim \mathcal{N}(\mathbf{0}, \mathbf{S}_t)$. This equation can be expanded to

$$\begin{aligned} \tilde{\mathbf{y}}_{t,1}^{**} &= (\mathbf{y}_t^{(1)})' \mathbf{d}_1 + \mathbf{u}_{t,1}, \\ \tilde{\mathbf{y}}_{t,1}^{**} &= h_{2,1} (\mathbf{y}_t^{(1)})' \mathbf{d}_1 + (\mathbf{y}_t^{(2)})' \mathbf{d}_2 + \mathbf{u}_{t,2}, \\ &\vdots \\ \tilde{\mathbf{y}}_{t,N}^{**} &= h_{N,1} (\mathbf{y}_t^{(1)})' \mathbf{d}_1 + \dots + h_{N,N-1} (\mathbf{y}_t^{(N-1)})' \mathbf{d}_{N-1} + (\mathbf{y}_t^{(N)})' \mathbf{d}_N + \mathbf{u}_{t,N}, \end{aligned} \quad (\text{B.4})$$

where $\mathbf{y}_t^{(j)}$ is a vector that contains the P lagged values of $\mathbf{y}_{t,j}$, $\mathbf{d}_j = (d_{j,1}, \dots, d_{j,P})'$, for $j = 1, \dots, N$, $h_{i,j}$ is the (i, j) entry of \mathbf{H} .

It is noteworthy that (B.4) is similar to Equation (12) in [Carriero et al. \(2022\)](#). An important difference is that they multiplied the same \mathbf{x}_t to each row of the coefficient matrix, whereas we multiply $(\mathbf{y}_t^{(j)})'$ to each \mathbf{d}_j . After slightly modifying Equations (13) - (15) in [Carriero et al. \(2022\)](#), we get the full conditional posterior $\mathbf{d}_j \mid \mathbf{B}_1, \mathbf{B}_2, \mathbf{B}_3, \mathbf{d}_{-j}, \mathbf{H}, \mathbf{S}_{1:T} \sim \mathcal{N}(\bar{\boldsymbol{\mu}}_{\mathbf{d}_j}, \bar{\boldsymbol{\Sigma}}_{\mathbf{d}_j})$, with

$$\bar{\boldsymbol{\Sigma}}_{\mathbf{d}_j}^{-1} = \boldsymbol{\Sigma}_{\mathbf{d}_j}^{-1} + \sum_{i=j}^N h_{i,j}^2 \sum_{t=1}^T s_{t,i}^{-1} \mathbf{y}_t^{(j)} (\mathbf{y}_t^{(j)})', \quad (\text{B.5})$$

$$\bar{\boldsymbol{\mu}}_{\mathbf{d}_j} = \bar{\boldsymbol{\Sigma}}_{\mathbf{d}_j} \left(\sum_{i=j}^N h_{i,j}^2 \sum_{t=1}^T s_{t,i}^{-1} \mathbf{z}_{t,i}^{(j)} \mathbf{y}_t^{(j)} \right), \quad (\text{B.6})$$

where $\mathbf{z}_{t,j+l}^{(j)} = \tilde{\mathbf{y}}_{t,j+l}^{**} - \sum_{i \neq j, i=1}^{j+l} h_{j+l,i} (\mathbf{y}_t^{(i)})' \mathbf{d}_i$, \mathbf{d}_{-j} represents \mathbf{D} without \mathbf{d}_j , $\boldsymbol{\Sigma}_{\mathbf{d}_j}$ is the prior covariance matrix of \mathbf{d}_j .

A more efficient way is to rewrite the system in (B.4) to

$$\left(\mathbf{Y}^{**} - \mathbf{X} \left(\mathbf{D}^{[j=0]} \right)' \right) \mathbf{H}'_{j:N,1:N} = \mathbf{Y}^{(j)} \mathbf{d}_j \mathbf{H}'_{j:N,k} + \mathbf{U}_{j:N}, \quad (\text{B.7})$$

where $\mathbf{Y}^{**} = (\mathbf{y}_1^{**}, \dots, \mathbf{y}_T^{**})'$, $\mathbf{X} = (\mathbf{x}_1, \dots, \mathbf{x}_T)'$, $\mathbf{H}_{j:N,1:N}$ is the block of \mathbf{H} composed of j - to N -th rows and all N columns, $\mathbf{Y}^{(j)} = (\mathbf{y}_1^{(j)}, \dots, \mathbf{y}_T^{(j)})'$, $\mathbf{D}^{[j=0]}$ is the same as \mathbf{D} except the j -th row as zeros, $\mathbf{U}_{j:N} = (\mathbf{u}_{1,j:N}, \dots, \mathbf{u}_{T,j:N})'$.

If we vectorize both sides of (B.7), the new equation is

$$\text{vec} \left(\left(\mathbf{Y}^{**} - \mathbf{X} \left(\mathbf{D}^{[j=0]} \right)' \right) \mathbf{H}'_{j:N,1:N} \right) = \left(\mathbf{H}_{j:N,k} \otimes \mathbf{Y}^{(j)} \right) \mathbf{d}_j + \text{vec} \left(\mathbf{U}_{j:N} \right).$$

Let

$$\begin{aligned} \tilde{\mathbf{Y}}^{(j)} &= \text{vec} \left(\left(\mathbf{Y}^{**} - \mathbf{X} \left(\mathbf{D}^{[j=0]} \right)' \right) \mathbf{H}'_{j:N,1:N} \right) ./ \text{vec} \left(\mathbf{S}_{1:T,k:N}^{1/2} \right) \\ \tilde{\mathbf{X}}^{(j)} &= \left(\mathbf{H}_{j:N,k} \otimes \mathbf{Y}^{(j)} \right) ./ \text{vec} \left(\mathbf{S}_{1:T,j:N}^{1/2} \right), \end{aligned}$$

where $./$ is Matlab element-by-element division operation, $\mathbf{S}_{1:T,j:N}$ is a T -by- $(N-J+1)$ matrix with the t -th row has entries $(s_{t,j}, \dots, s_{t,N})$.

Then (B.5) and (B.6) are simplified to

$$\bar{\Sigma}_{d_j}^{-1} = \underline{\Sigma}_{d_j}^{-1} + \left(\tilde{\mathbf{X}}^{(j)} \right)' \tilde{\mathbf{X}}^{(j)} \quad (\text{B.8})$$

$$\bar{\boldsymbol{\mu}}_{d_j} = \bar{\Sigma}_{d_j} \left(\tilde{\mathbf{X}}^{(j)} \right)' \tilde{\mathbf{Y}}^{(j)}. \quad (\text{B.9})$$

B.2 Full Conditionals Related to Multiplicative Gamma Prior

Posteriors of hyperparameters in the MGP are similar to those in [Bhattacharya and Dunson \(2011\)](#).

Since $\phi_{(r,j,i_j)}$ is a local hyperparameter of $\boldsymbol{\beta}_{j,i_j}^{(r)}$, the derivation of its conditional posterior given $\boldsymbol{\beta}_{j,i_j}^{(r)}$ and τ_r is

$$\begin{aligned} p\left(\phi_{(r,j,i_j)} \mid \boldsymbol{\beta}_{j,i_j}^{(r)}, \tau_r\right) &\propto \left(\phi_{(r,j,i_j)}^{-1}\right)^{-1/2} \exp\left(-\frac{\left(\boldsymbol{\beta}_{j,i_j}^{(r)}\right)^2}{2\phi_{(r,j,i_j)}^{-1}\tau_r^{-1}}\right) \left(\phi_{(r,j,i_j)}\right)^{\frac{\nu}{2}-1} \exp\left(-\frac{\nu}{2}\phi_{(r,j,i_j)}\right) \\ &= \left(\phi_{(r,j,i_j)}\right)^{\frac{\nu+1}{2}-1} \exp\left(-\frac{\tau_r\left(\boldsymbol{\beta}_{j,i_j}^{(r)}\right)^2 + \nu}{2}\phi_{(r,j,i_j)}\right). \end{aligned}$$

Thus, the conditional posterior of $\phi_{(r,j,i_j)}$ is a Gamma distribution

$$\phi_{(r,j,i_j)} \mid \boldsymbol{\beta}_{j,i_j}^{(r)}, \tau_r \sim \text{Gamma}\left(\frac{\nu+1}{2}, \frac{\nu + \tau_r\left(\boldsymbol{\beta}_{j,i_j}^{(r)}\right)^2}{2}\right).$$

δ_1 involves in all τ_r 's, for $r = 1, \dots, R$, so the sampling δ_1 is conditional to all margins and corresponding hyperparameters, denoted as \cdot . Combining likelihood and prior, we get

$$\begin{aligned} p(\delta_1 \mid \cdot) &\propto \delta_1^{a_1-1} \exp(-\delta_1) \prod_{r=1}^R \prod_{j=1}^3 \prod_{i_j=1}^{I_j} \delta_1^{\frac{1}{2}} \exp\left(-\frac{\phi_{(r,j,k)}\delta_1\tau_l^{(1)}\left(\boldsymbol{\beta}_{j,i_j}^{(r)}\right)^2}{2}\right) \\ &= \delta_1^{a_1 + \frac{(2N+P)R}{2} - 1} \exp\left(-\left(1 + \sum_{r=1}^R \tau_l^{(1)} \sum_{j=1}^3 \sum_{i_j=1}^{I_j} \frac{\phi_{(r,j,i_j)}\left(\boldsymbol{\beta}_{j,i_j}^{(r)}\right)^2}{2}\right)\delta_1\right), \end{aligned} \quad (\text{B.10})$$

where $\tau_l^{(r)} = \prod_{i=1, i \neq r}^l \delta_i$, p_j is the number of rows in \mathbf{B}_j .

The derivation leads to a Gamma conditional posterior of δ_1

$$\delta_1 \mid \cdot \sim \text{Gamma}\left(a_1 + \frac{(2N+P)R}{2}, 1 + \frac{1}{2} \sum_{l=1}^R \tau_l^{(1)} \sum_{d=1}^3 \sum_{k=1}^{p_j} \phi_{(r,j,i_j)}\left(\boldsymbol{\beta}_{j,i_j}^{(l)}\right)^2\right).$$

The derivation of the conditional posterior of δ_r , for $r > 1$, is similar to the above derivation, but the prior and likelihood are slightly different. We first need to change a_1 in [B.10](#) to a_2 , and since δ_r is only related to $\boldsymbol{\beta}_{j,i_j}^{(l)}$'s and their corresponding hyperparameters, where $l \geq r$, the starting value of l

is r rather than 1, and we amend $\tau_l^{(1)}$ to $\tau_l^{(r)}$. This results to a Gamma conditional posterior of δ_r

$$\delta_r \mid \cdot \sim \text{Gamma} \left(a_2 + \frac{(2N + P)(R - r + 1)}{2}, 1 + \frac{1}{2} \sum_{l=r}^R \tau_l^{(r)} \sum_{d=1}^3 \sum_{i_j=1}^{p_j} \phi_{(r,j,i_j)}(\beta_{j,i_j}^{(l)})^2 \right),$$

where we keep \cdot as conditions for brevity. τ_r is updated as the product of $\delta_1, \dots, \delta_r$ in each iteration.

B.3 Details for Other Full Conditionals

Conditional posteriors related to the normal-gamma prior (hyperparameters of \mathbf{D} and \mathbf{H}) are almost identical to those in [Huber and Feldkircher \(2019\)](#). The only difference is that these posteriors are conditional on entries of \mathbf{D} and \mathbf{H} , instead of the coefficient matrix.

The conditional posterior of \mathbf{H} can also be found in [Huber and Feldkircher \(2019\)](#). For stochastic volatility, we use an ASIS algorithm proposed in [Kastner and Frühwirth-Schnatter \(2014\)](#) and implement it with an R package called **stochvol** ([Kastner, 2016](#)).

C Algorithms

C.1 Full Gibbs Sampler

Algorithm 1 Initialize unknown parameters and repeat the following steps in each iteration:

Step (a): Update $\mathbf{B}_1^{\text{old}}$ under the base parameterization.

Step (b*): Store the first row of $\mathbf{B}_1^{\text{old}}$ into \mathbf{D}_1 and determine $\mathbf{B}_1^*, \mathbf{B}_2^*$.

Step (b**): Sample $(\beta_{1,1}^{\text{new}(r)})^2$ for $r = 1, \dots, R$ using the second parameterization and store corresponding values in \mathbf{D}_1 .

Step (b***): Update $\mathbf{B}_1^{\text{new}}$ and $\mathbf{B}_2^{\text{new}}$ with transformation

$$\mathbf{B}_1^{\text{new}} = \mathbf{B}_1^* \mathbf{D}_1, \mathbf{B}_2^{\text{new}} = \mathbf{B}_2^* \mathbf{D}_1^{-1}.$$

Step (c): Update $\mathbf{B}_2^{\text{old}}$ under the base parameterization.

Step (d*): Store the first row of $\mathbf{B}_2^{\text{old}}$ into \mathbf{D}_2 and determine $\mathbf{B}_2^*, \mathbf{B}_3^*$.

Step (d**): Sample $(\beta_{2,1}^{\text{new}(r)})^2$ for $r = 1, \dots, R$ using the third parameterization and store corresponding values in D_2 .

Step (d***): Update B_2^{new} and B_3^{new} with transformation

$$B_2^{\text{new}} = B_2^{**} D_2, B_3^{\text{new}} = B_3^{**} D_2^{-1}.$$

Step (e): Update B_3^{old} under the base parameterization.

Step (f*): Store the first row of B_3^{old} into D_3 and determine B_3^{***}, B_1^{***} .

Step (f**): Sample $(\beta_{3,1}^{\text{new}(r)})^2$ for $r = 1, \dots, R$ using the fourth parameterization and store corresponding values in D_3 .

Step (f***): Update B_3^{new} and B_1^{new} with transformation

$$B_3^{\text{new}} = B_3^{***} D_3, B_1^{\text{new}} = B_1^{***} D_3^{-1}.$$

Step (g): Sample other unknown parameters from their full conditionals.

C.2 Post-processing Procedure

The interweaving strategy only improves the mixing of entries in B up to column permutations and sign-switching issues. The method proposed to solve these problems is inspired by the Match-Sign-Factor (MSF) algorithm in the R package **infinitefactor** (Poworoznek et al., 2021). The MSF performs a greedy search to rotate factor loadings and factors in factor models, and we apply a variant of this algorithm to Tensor VARs. Our algorithm is presented in 4, along with a detailed explanation divided into two parts: (1) solve column permutations by the label-matching method; (2) solve sign-switching issues by the sign-matching method.

Column permutations in B are equivalent to those in B_3 , so if we solve the equivalent issue in B_3 , we will automatically solve column permutations in B . There are analogous equivalences related to B_1 and B_2 , but the empirical finding in Figure 9 shows that the label matching related to B_3 gives the best mixing results in the simulation study. We will discuss the possible explanation for

this finding after describing the method in detail. The label matching needs a *pivot* matrix $\mathbf{B}_3^{(\text{pivot})}$ as a template to align \mathbf{B}_3 sampled in each iteration, i.e. columns in \mathbf{B}_3 after label being matched will have the same order as that of columns in $\mathbf{B}_3^{(\text{pivot})}$. Following Poworoznek et al. (2021), $\mathbf{B}_3^{(\text{pivot})}$ is the one with the median of the condition number $\kappa = \sigma_{\max}(\mathbf{B}_3)$, where $\sigma_{\max}(\mathbf{B}_3)$ is the maximal singular value of \mathbf{B}_3 .

After choosing the pivot, we compute the Euclidean distance between columns in \mathbf{B}_3 in each iteration and $(\mathbf{B}_3^{(\text{pivot})}, -\mathbf{B}_3^{(\text{pivot})})$, and store the distances into an R -by- $2R$ distance matrix Θ with row and column indices corresponding to columns in \mathbf{B}_3 and $(\mathbf{B}_3^{(\text{pivot})}, -\mathbf{B}_3^{(\text{pivot})})$, respectively. As shown in Algorithm 4, a greedy algorithm then starts from the lowest Euclidean distance to align the corresponding column in \mathbf{B}_3 to that in $\mathbf{B}_3^{(\text{pivot})}$ or $-\mathbf{B}_3^{(\text{pivot})}$, and these columns will not be matched again. The label matching is finished after repeating the procedure for R times.

As mentioned earlier, regarding samples of \mathbf{B}_3 as candidates for the pivot matrix, rather than \mathbf{B}_1 , \mathbf{B}_2 and \mathbf{B} , leads to empirically the best mixing results of margins. Note that numbers of rows in \mathbf{B}_1 , \mathbf{B}_2 , \mathbf{B}_3 and \mathbf{B} are N , N , P , $2N+P$, respectively. One possible reason for this best performance of using \mathbf{B}_3 is that N and $2N+P$ are greater than P in our simulation and real data experiments, so it is easier to correctly match columns in \mathbf{B}_3 to those in $\mathbf{B}_3^{\text{pivot}}$, compared to similar procedures using \mathbf{B}_1 , \mathbf{B}_2 and \mathbf{B} .

Next, we explain the second part about the sign-matching method. For $j = 1, 2$, $r = 1, \dots, R$, we determine whether to flip the sign of $\mathbf{B}_{j,(\cdot,r)}$ by comparing its distances to both $\mathbf{B}_{j,(\cdot,r)}^{(\text{pivot})}$ and $-\mathbf{B}_{j,(\cdot,r)}^{(\text{pivot})}$. The general guideline for flipping signs in $\mathbf{B}_{3,(\cdot,r)}$ is to do so only if this procedure identifies the tensor, i.e. the tensors before and after sign-matching are the same. If not, we leave the sign unflipped.

Algorithm 4 Match Labels and Signs

Find a pivot matrix $\mathbf{B}_3^{(\text{pivot})}$ and its corresponding tensor matrix $\mathbf{B}^{(\text{pivot})}$

for each iteration **do**

 Compute the R -by- $2R$ distance matrix Θ

for $r = 1, \dots, R$ **do**

Find $(r_1^*, r_2^*) = \operatorname{argmin}_{r_1, r_2} \Theta_{r_1, r_2}$

if $r_2^* \leq R$ **then**

Match the r_1^* -th column in \mathbf{B}_3 to the r_2^* -th column in $\mathbf{B}_3^{(\text{pivot})}$.

Change the r_1 -th row, r_2 -th and $(R + r_2)$ -th columns in Θ to infinity.

else

Match the r_1^* -th column in \mathbf{B} to the $(r_2^* - R)$ -th column in $\mathbf{B}_3^{(\text{pivot})}$.

Change the r_1 -th row, $(r_2 - R)$ -th and r_2 -th columns in Θ to infinity.

for $j = 1, 2$ **do**

Compute distance $d_1 = d(\mathbf{B}_{j,(\cdot,r)}, \mathbf{B}_{j,(\cdot,r)}^{(\text{pivot})})$ and $d_2 = d(\mathbf{B}_{j,(\cdot,r)}, -\mathbf{B}_{j,(\cdot,r)}^{(\text{pivot})})$

if $d_1 \leq d_2$ **then**

Keep signs in $\mathbf{B}_{j,(\cdot,r)}$. Record $\text{ind}_{j,r} = 1$

else

Flip signs in $\mathbf{B}_{j,(\cdot,r)}$. Record $\text{ind}_{j,r} = -1$

if $\text{ind}_{1,r} \text{ind}_{2,r} = 1$ **then**

Keep the signs in $\mathbf{B}_{3,(\cdot,r)}$

else

Flip the signs in $\mathbf{B}_{3,(\cdot,r)}$

D Additional Results

D.1 Additional Results in Simulation Study

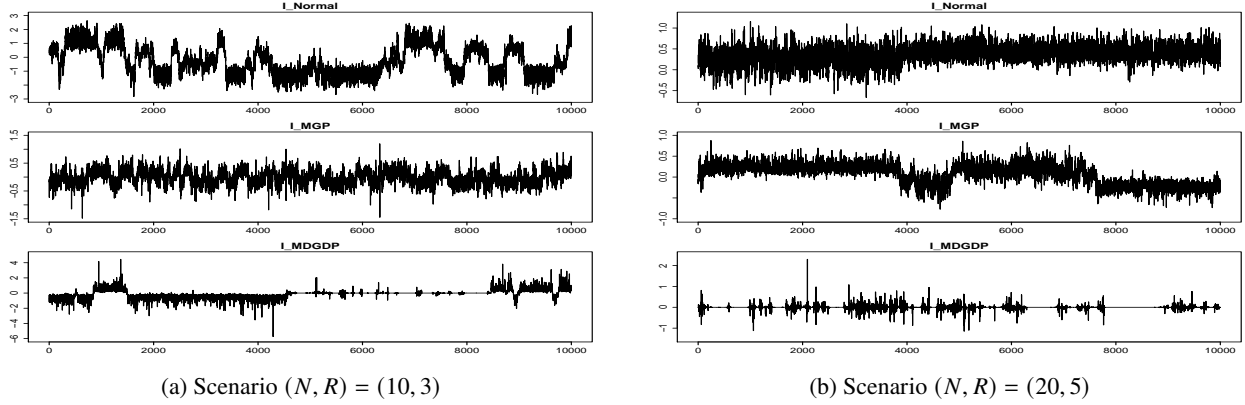


Figure 8: Trace plots of $\beta_{1,1}^{(1)}$ in $N = 10, R = 3$ scenario (left) and $\beta_{1,2}^{(1)}$ in $N = 20, R = 5$ scenario (right) after burn-in period. The inferential scheme adopts standard normal (top), MGP (middle) and M-DGDP (bottom) as priors and applies with the interweaving strategy. The figure shows the necessity of the column- and sign-matching method.

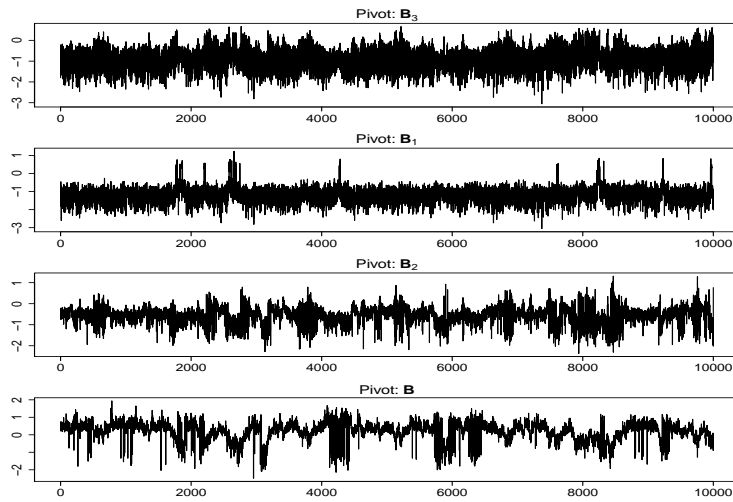


Figure 9: Trace plots of the first 10,000 draws of $\beta_{1,1}^{(1)}$ in $N = 10, R = 3$ scenario after burn-in period. The inferential scheme adopts standard normal prior with interweaving strategy, and the post-processing procedure in each panel chooses different pivot indicated in the title.

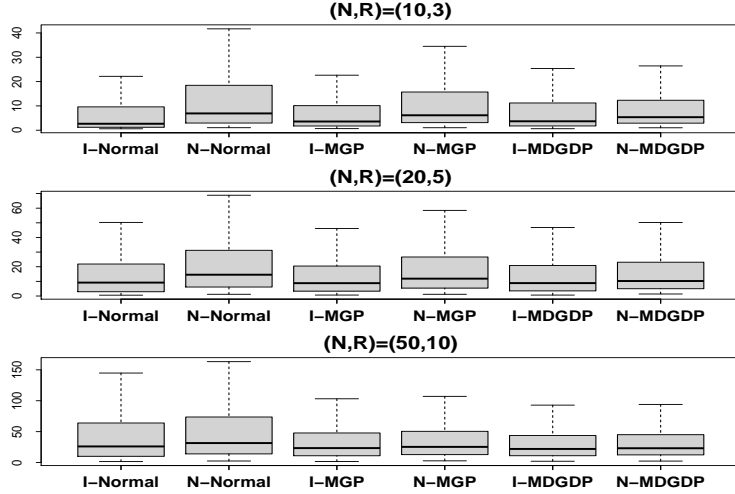


Figure 10: Boxplots of inefficiency factors of coefficient matrices from different scenarios: $(N, R) = (10, 3)$ (top), $(N, R) = (20, 5)$ (middle) and $(N, R) = (50, 10)$ (bottom). Inferential schemes with and without interweaving are represented as "I-" and "N-", respectively, followed by a prior setting. Outliers are discarded.

D.2 Additional Results in Real Data Application

Model	Horizon	MSFE							
		Joint	RPI	CPIAUCSL	GDP	FEDFUNDS	UNRATE	GDPDEFL	GS10
Tensor MGP	1	0.710	0.900	1.022	0.444	0.202	0.413	0.597	0.772
	2	0.771	0.951	1.207	0.511	0.224	0.518	0.609	0.785
	4	0.834	1.055	1.225	0.585	0.243	0.647	0.573	0.760
tensor MPG Own-Lag	1	0.672	0.942	0.967	0.417	0.178	0.385	0.472	0.762
	2	0.768	0.942	1.207	0.464	0.235	0.534	0.613	0.769
	4	0.833	1.055	1.225	0.539	0.246	0.689	0.585	0.754
Minnesota	1	0.689	1.041	0.970	0.354	0.190	0.344	0.485	0.801
	2	0.806	1.014	1.227	0.437	0.268	0.481	0.673	0.880
	4	0.883	1.123	1.219	0.528	0.271	0.641	0.636	0.891
SSVS	1	0.746	1.143	1.082	0.403	0.308	0.445	0.531	0.805
	2	0.853	1.091	1.332	0.577	0.413	0.663	0.662	0.859
	4	0.925	1.260	1.215	0.630	0.333	0.856	0.680	0.810
NG	1	0.740	0.964	1.052	0.515	0.198	0.507	0.573	0.763
	2	0.803	1.000	1.218	0.580	0.234	0.637	0.615	0.772
	4	0.852	1.095	1.221	0.614	0.241	0.719	0.584	0.754

Table 7: MSFE of joint and marginal variables using the medium-scale data set. The best forecasts are in bold.

Model	Horizon	MSFE							
		Joint	RPI	CPIAUCSL	GDP	FEDFUNDS	UNRATE	GDPDEFL	GS10
tensor MGP	1	0.753	0.911	0.942	0.483	0.192	0.533	0.618	0.768
	2	0.795	0.969	1.177	0.524	0.211	0.608	0.603	0.773
	4	0.829	1.053	1.241	0.577	0.240	0.684	0.575	0.756
tensor MPG Own-Lag	1	0.681	0.968	0.922	0.427	0.180	0.378	0.483	0.788
	2	0.781	0.966	1.186	0.477	0.228	0.542	0.610	0.779
	4	0.819	1.060	1.229	0.555	0.241	0.664	0.577	0.759
Minnesota	1	0.800	1.063	0.979	0.382	0.215	0.361	0.551	1.250
	2	1.036	1.066	1.221	0.477	0.343	0.519	0.690	1.512
	4	1.334	1.263	1.254	0.621	0.415	0.802	0.650	1.757
SSVS	1	0.677	1.377	0.948	0.424	0.131	0.351	0.554	0.773
	2	0.786	1.331	1.203	0.537	0.208	0.507	0.666	0.776
	4	0.836	1.694	1.240	0.603	0.236	0.663	0.593	0.763
NG	1	0.791	0.958	1.133	0.631	0.194	0.617	0.614	0.772
	2	0.815	0.997	1.211	0.647	0.228	0.654	0.604	0.775
	4	0.834	1.076	1.236	0.638	0.241	0.700	0.577	0.759

Table 8: MSFE of joint and marginal variables using the large-scale data set. The best forecasts are in bold.

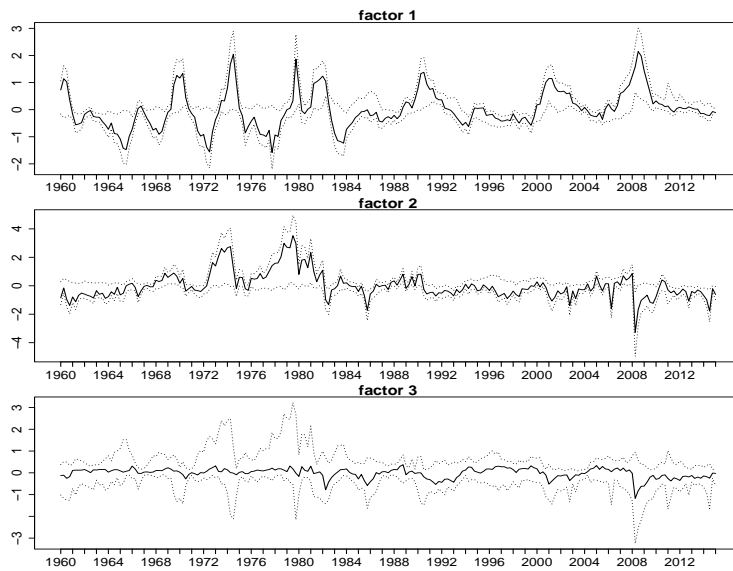


Figure 11: Time series plots of factors with median (solid line) and 80% credible interval (dashed line). The model does not include an own-lag matrix.

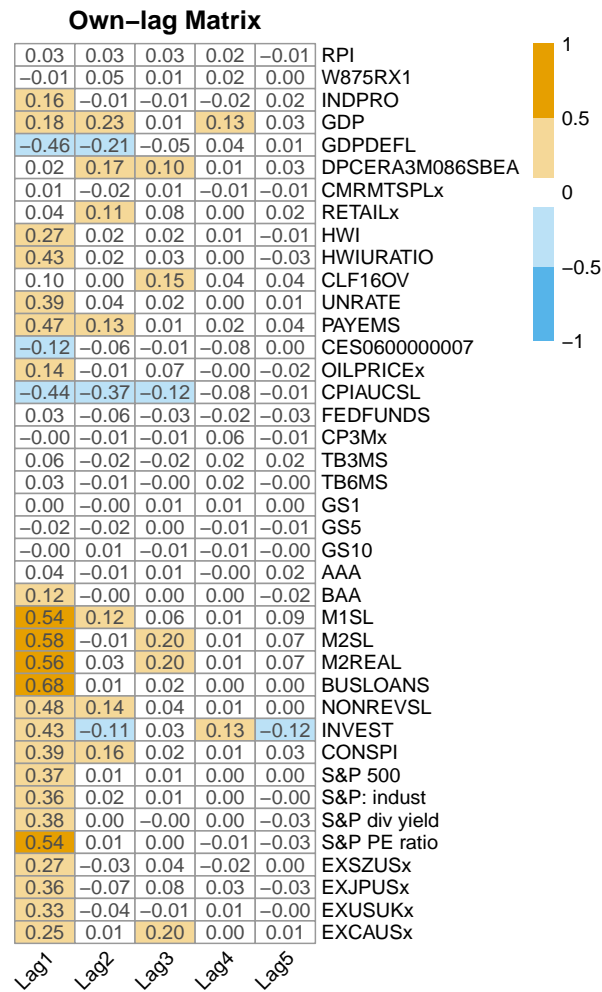


Figure 12: Posterior mean of non-zero entries in the own-lag matrix inferred using the large-scale data set. Each row correspond to a variable and each column is for a lag order.

E Data

Slow Variables

	Name	Description	Medium	Large	Category	Transformation
1	RPI	Real Personal Income	x	x	1	5
2	W875RX1	RPI ex. Transfers	x	x	1	5
3	INDPRO	IP Index		x	1	5
4	GDP	Real Gross Domestic Product	x	x	1	5
5	GDPDEFL	GDP deflator	x	x	1	6
6	DPCERA3M086SBEA	Real PCE	x	x	2	5
7	CMRMTSPLx	Real M& T Sales	x	x	2	5
8	RETAILx	Retail and Food Services Sales	x	x	2	5
9	HWI	Help-Wanted Index for US		x	3	2
10	HWIURATIO	Help Wanted to Unemployed ratio		x	3	2
11	CLF16OV	Civilian Labor Force		x	3	5
12	UNRATE	Civilian Unemployment Rate	x	x	3	2
13	PAYEMS"	All Employees: Total nonfarm	x	x	3	5
14	CES0600000007	Hours: Goods-Producing		x	3	5
15	OILPRICEx	Crude Oil Prices: WTI		x	4	5
16	CPIAUCSL	CPI: All Items	x	x	4	6

Fast Variables

	Name	Description	Medium	Large	Category	Transformation
17	FEDFUNDS	Effective Federal Funds Rate	x	x	5	2
18	CP3Mx	3-Month AA Comm. Paper Rate	x	x	5	2
19	TB3MS	3-Month T-bill		x	5	2
20	TB6MS	6-Month T-bill		x	5	2
21	GS1	1-Year T-bond		x	5	2
22	GS5	5-Year T-bond		x	5	2
23	GS10	10-Year T-bond	x	x	5	2
24	AAA	Aaa Corporate Bond Yield		x	5	2
25	BAA	Baa Corporate Bond Yield		x	5	2

26	M1SL	M1 Money Stock		x	6	5
27	M2SL	M2 Money Stock		x	6	5
28	M2REAL	Real M2 Money Stock		x	6	5
29	BUSLOANS	Commercial and Industrial Loans	x	x	6	5
30	NONREVSL	Total Nonrevolving Credit	x	x	6	5
31	INVEST	Securities in Bank Credit		x	6	5
32	CONSPI	Credit to PI ratio	x	x	6	2
33	S&P 500	S&P 500		x	7	5
34	S&P: indust	S&P Industrial		x	7	5
35	S&P div yield	S&P Divident yield		x	7	2
36	S&P PE ratio	S&P Price/Earnings ratio		x	7	5
37	EXSZUSx	Switzerland / U.S. FX Rate	x	x	8	5
38	EXJPUSx	Japan / U.S. FX Rate	x	x	8	5
39	EXUSUKx	U.S. / U.K. FX Rate	x	x	8	5
40	EXCAUSx	Canada / U.S. FX Rate	x	x	8	5

Transformation code: 2 - first differences; 5 - first differences of logarithms; 6 - second differences of logarithms.

Table 9: Data description.